

A Study on Longevity Risk Hedging in the Presence of Population Basis Risk

by

Kenneth Qian Zhou

A thesis
presented to the University of Waterloo
in fulfillment of the
thesis requirement for the degree of
Master of Mathematics
in
Actuarial Science

Waterloo, Ontario, Canada, 2015

© Kenneth Qian Zhou 2015

I hereby declare that I am the sole author of this thesis. This is a true copy of the thesis, including any required final revisions, as accepted by my examiners.

I understand that my thesis may be made electronically available to the public.

Abstract

Longevity risk refers to uncertainty surrounding the trend in human life expectancy. Standardized hedging instruments that are linked to broad-based mortality indexes can be used to offload longevity risk from pension plans and annuities. However, hedges that are based on such instruments are subject to population basis risk, which arises from the difference in mortality improvements between the hedger's population and the reference population to which the hedging instruments are linked. This thesis attempts to address some issues that are related to longevity risk hedging in the presence of population basis risk.

In the first chapter, a graphical risk metric is proposed to intuitively measure population basis risk, which is believed to be a major obstacle to market development. It allows market participants to not only visually evaluate the extent of population basis risk, but also determine the most appropriate reference population. Compared to existing population basis risk metrics which are mostly numerical, the proposed graphical risk metric is more informative in that it captures more aspects of population basis risk. Along with the existing numerical risk metrics, the proposed graphical risk metric may help hedgers better understand population basis risk and hence make their risk management decisions.

In the second chapter, the feasibility of dynamic longevity hedging with standardized hedging instruments is studied. To this end, the dynamic hedging strategy developed by Cairns (2011) is generalized to incorporate the situation when the hedger's population and the reference population are different. The empirical results indicate that dynamic hedging can effectively reduce the longevity risk exposures of a typical pension plan, even if population basis risk is taken into account. Further, by considering data from a large

group of national populations, it is found that population basis risk and small sample risk can possibly be diversified across different hedgers. Hedgers may therefore be able to completely eliminate their longevity risk exposures by removing the underlying trend risk with a dynamic index-based hedge and transferring the residual risks through a reinsurance mechanism.

Acknowledgements

I would like to express my deepest gratitude to my supervisor, Professor Johnny Li, who has inspired, guided and helped me through my master's studies with his insightful ideas and unreserved support. I would also like to thank Professors Mary Hardy and Jun Cai for their time and effort in examining this thesis. Special thanks also to Professors Wai-Sum Chan and Rui Zhou for their constructive suggestions. I would like to acknowledge the Department of Statistics and Actuarial Science's funding support, and Ms. Mary Lou Dufton's assistance. Finally, I would like to express my appreciation to Cynthia McLauchlan, who has spent endless amounts of time encouraging and supporting me.

Dedication

This thesis is dedicated to my parents for their limitless love, support and encouragement.

Table of Contents

List of Tables	x
List of Figures	xi
1 Towards a Large and Liquid Longevity Market: A Graphical Population Basis Risk Metric	1
1.1 Introduction	1
1.2 Methodology	3
1.3 An Illustration	6
1.4 Conclusion	11
2 Dynamic Longevity Hedging in the Presence of Population Basis Risk: A Feasibility Analysis from Technical and Economic Perspectives	15
2.1 Introduction	15
2.2 The Dynamic Longevity Hedging Strategy	22

2.2.1	The Assumed Model	22
2.2.2	The Set-up	24
2.2.3	The Approximation Methods	27
2.2.4	Deriving Hedge Ratios	30
2.2.5	Evaluating the Hedge	31
2.3	Analyzing the Dynamic Longevity Hedge	33
2.3.1	Assumptions	33
2.3.2	Baseline Results	35
2.3.3	Robustness	39
2.4	Managing the Residual Risks	51
2.4.1	Assumptions	53
2.4.2	An Exploratory Analysis	55
2.4.3	A Customized Surplus Swap	57
2.4.4	An Illustration	63
2.5	Discussion and Conclusion	67
	Appendices	71
	A Evaluating the Quality of the Approximation Methods	72
	B Deriving the Approximation Formula for $p_{x,u}^{(i)}(T, K_t, k_t^{(i)})$ when $u > t$	77

List of Tables

1.1	The calculated values of $h^{(R)}$	9
2.1	The name and index of the 25 male populations	54
2.2	The sample correlation coefficients of the log central death rates for the 25 male populations	58
2.3	The sample correlation coefficients of the log central death rates without the common time trend for the 25 male populations	59

List of Figures

1.1	The graphical risk metric for one reference population	13
1.2	The graphical risk metric for four reference populations	14
2.1	A graphical illustration of the proposed hedging framework	21
2.2	The distributions of the partial derivatives of FL_t and $Q_t(t)$, and h_t	36
2.3	The distributions of the liabilities when population basis risk is present	38
2.4	The values of the hedge effectiveness over time	40
2.5	The distributions of the liabilities when population basis risk is absent	41
2.6	The distributions of the liabilities when model risk is present	45
2.7	The distributions of the liabilities when small sample risk is present	48
2.8	The distributions of the liabilities when using q-forwards with different reference ages	50
2.9	The distributions of the liabilities when using q-forwards with different time-to-maturities	52

2.10	The distributions of the liabilities for the 25 pension plans	56
2.11	An illustration of the cash exchange of a customized surplus swap	62
2.12	The distributions of the net cash flows of the customized surplus swap for the 25 pension plans	64
2.13	The distributions of the average net cash flows	65
2.14	The variances of the average net cash flows and the individual net cash flows	66
A.1	The degrees of accuracy in estimating $p_{x_0,t}^{(H)}(s, K_t, k_t^{(H)})$	75
A.2	The degrees of accuracy in estimating $p_{x_f, t_0+T^*-1}^{(R)}(1, K_t, k_t^{(R)})$	76

Chapter 1

Towards a Large and Liquid Longevity Market: A Graphical Population Basis Risk Metric

1.1 Introduction

Rapid, unexpected increases in human life expectancy have posed what is known as longevity risk. On a macroeconomic level, longevity risk affects current account (Lee and Mason, 2010), GDP (Skirbekk, 2004), and productivity (van Groezen et al., 2005). From a microeconomic viewpoint, longevity risk undermines the profits and growth opportunities of corporations offering defined-benefit pension schemes, ultimately affecting their share prices. According to the International Monetary Fund (2012), if individuals live three years

longer than expected, then the already large pension costs would increase by 50% of the 2010 GDP in advanced economies and 25% of the 2010 GDP in emerging economies.

Recently, some pension plan sponsors and annuity providers have chosen to offload longevity risk from their balance sheets. One way to accomplish this act is by transferring the risk to capital markets, through standardized derivative securities that are linked to broad-based mortality indexes. The first of such transactions occurred in 2008 when Lucida PLC passed part of its longevity risk exposure onto J.P. Morgan by means of a mortality q-forward contract. The risk was subsequently transferred to various institutional investors, who accepted the risk exposure for a risk premium (Blake et al., 2013). Compared to other risk transfer methods such as reinsurance, capital markets solutions are advantageous in terms of being less costly and having, in theory, no capacity constraint (Cummins and Trainar, 2009).

Nevertheless, at this point the market for standardized mortality-linked securities is small and lacks liquidity. The industry leaders believe that one major obstacle to market development is an inadequate understanding of population basis risk, the residual risk that originates from the difference in mortality improvements between the hedger's population and the reference population to which the hedging instrument is linked (Life and Longevity Markets Association (LLMA), 2012). This problem has been studied by several researchers, who quantified the risk by numerical metrics including percentage reduction in expected shortfall (Ngai and Sherris, 2011), percentage reduction in variance (Cairns et al., 2014; Li and Hardy, 2011; Li and Luo, 2012), and minimal required buffer (Stevens et al., 2011).¹

¹The minimal required buffer refers to the minimum asset value (in excess of the best estimate value of the liabilities) such that the probability that the insurer or pension fund will be able to pay all future liabilities is sufficiently high.

However, as the existing methods cannot be easily communicated to market participants, they still cannot meet the industry's need for a simple, intuitive metric for population basis risk.

To aid in filling this gap, in this chapter we contribute a graphical risk metric for assessing population basis risk. The graphical risk metric is constructed from a series of joint prediction regions, allowing users to visually evaluate the ranges of possible outcomes at various confidence levels. Our contribution also enables hedgers to determine, out of all available reference populations, the population that results in the minimum amount of population basis risk. We believe that our contribution is likely to gain wide acceptance among practitioners, who are increasingly relying on graphical methods such as survivor fan charts (Blake et al., 2008), longevity fan charts (Dowd et al., 2010), and heat maps of mortality improvement rates (Continuous Mortality Investigation Bureau, 2009) in making their risk management decisions.

We explain the construction of the graphical population basis risk metric in the next section, followed by a section that includes a demonstration based on a hypothetical example and real mortality data. Finally the last section concludes the chapter with some suggestions for future research.

1.2 Methodology

Let us consider a pension plan whose liability value is proportional to a random survivor index, $S^{(H)}$, where H represents the population of individuals associated with the plan. To

hedge its longevity risk exposure, the plan trades a longevity-linked derivative, whose payoff is proportional to another random survivor index, $S^{(R)}$, where R denotes the derivative's reference population. We let $I^{(H)} = S^{(H)} - E(S^{(H)})$ and $I^{(R)} = S^{(R)} - E(S^{(R)})$ be the exceedances of $S^{(H)}$ and $S^{(R)}$ over their expected values, respectively. We base the graphical risk metric on $I^{(H)}$ and $I^{(R)}$ rather than $S^{(H)}$ and $S^{(R)}$, partly because users' primary interest are the possible deviations from the expected outcomes, and partly because the use of $I^{(H)}$ and $I^{(R)}$ ensures all resulting risk metrics are centered at the origin, thereby allowing users to compare the risk metrics for different reference populations readily.

The first step in constructing the graphical population basis risk metric is to simulate realizations of $I^{(H)}$ and $I^{(R)}$ from a multi-population stochastic mortality model, examples of which include the augmented common factor model (Li and Lee, 2005) and the gravity model (Dowd et al., 2011). Such a model incorporates the correlation between the uncertain mortality improvements of the populations being modeled, and exhibits mean-reversion to avoid resulting in anti-intuitive diverging long-term mortality forecasts.

The second step is to optimize the longevity hedge. We consider a static hedge, which seems more feasible than a dynamic hedge in today's market for longevity risk transfers.² Specifically, we aim to find, per dollar amount of the pension liability, the notional amount $h^{(R)}$ of the longevity-linked derivative that would lead to a perfect hedge in the ideal situation when population basis risk is absent, i.e., when $I^{(H)}$ and $I^{(R)}$ are perfectly correlated. We find $h^{(R)}$ by a linear approximation, which implies $h^{(R)} = \frac{\partial I^{(H)}}{\partial I^{(R)}}$. The value of $h^{(R)}$ is estimated by the slope of the first order linear regression of $I^{(H)}$ on $I^{(R)}$, derived from the

²Static hedging is more realistic, because dynamic hedging requires liquid longevity-linked securities that are not yet available in the current market for longevity risk transfers. See Fung et al. (2014).

simulated values of $I^{(H)}$ and $I^{(R)}$ obtained in the first step.

Our choice of $h^{(R)}$, which can be expressed as

$$h^{(R)} = \frac{\text{Cov}(I^{(R)}, I^{(H)})}{\text{Var}(I^{(H)})},$$

is justified in the sense that it minimizes the variance of the hedged portfolio; that is, $h^{(R)}$ is the value of h that minimizes the following expression:

$$\begin{aligned} \text{Var}(I^{(H)} - hI^{(R)}) &= \text{Var}(I^{(H)}) + h^2\text{Var}(I^{(R)}) - 2h\text{Cov}(I^{(H)}, I^{(R)}) \\ &= \text{Var}(I^{(R)}) \left(h - \frac{\text{Cov}(I^{(H)}, I^{(R)})}{\text{Var}(I^{(R)})} \right)^2 + c, \end{aligned}$$

where c is a constant that is free of h .

Of course, when population basis risk is actually present in reality, $I^{(H)}$ is not necessarily equal to $h^{(R)}I^{(R)}$. If $I^{(H)} > h^{(R)}I^{(R)}$, then the pension liability is under-hedged, and if $I^{(H)} < h^{(R)}I^{(R)}$, then the opposite is true. Population basis risk can therefore be understood as the variability associated with the random deviations between $I^{(H)}$ and $h^{(R)}I^{(R)}$.

The third step is to express the uncertainty surrounding $I^{(H)}$ and $h^{(R)}I^{(R)}$ by a series of joint prediction regions. Mathematically, \mathbf{J}_α is a joint prediction region for the duplet $(I^{(H)}, h^{(R)}I^{(R)})$ with coverage probability $0 < 1 - \alpha \leq 1$ if

$$\Pr((I^{(H)}, h^{(R)}I^{(R)}) \in \mathbf{J}_\alpha) = 1 - \alpha.$$

The region \mathbf{J}_α should encompass $100(1 - \alpha)\%$ of the possible combinations of $I^{(H)}$ and

$h^{(R)}I^{(R)}$. For a given value of α , a larger \mathbf{J}_α reflects a higher amount of population basis risk. We construct nine joint prediction regions, with $\alpha = 0.1, 0.2, \dots, 0.9$.

Finally, the graphical risk metric is created by plotting on a Cartesian coordinate plane the 10% joint prediction region with the darkest shading, surrounded by the 20%, 30%, ..., 90% joint prediction regions with progressively lighter shadings. From the areas of the prediction regions and the degrees of shading, one can visualize ranges of possible hedging outcomes and their associated probabilities of occurrence. The proposed risk metric is somewhat similar to the well-known Bank of England inflation fan chart, which simultaneously depicts interval forecasts of future inflation rates at different confidence levels by using different shades of colour (Wallis, 2003). It also has a close resemblance to the existing survivor/longevity fan charts (Blake et al., 2008; Dowd et al., 2010).

1.3 An Illustration

We now illustrate the graphical population basis risk metric with a hypothetical example. Let us suppose that H , the population associated with the pension plan (the hedger), is Canadian males. Suppose further that at the time when the hedge is established, there is no longevity-linked derivative linked to Canadian males. However, the plan may use a longevity-linked derivative that is linked to an alternative reference population (R), which can be either U.S. males, German males, Dutch males, or English and Welsh males.³

The survivor index used is the *ex post* probability that an individual currently aged 65

³As a matter of fact, the LLMA provides mortality indexes for these four national populations. Derivative securities can be written on LLMA's mortality indexes.

will survive to age 90:

$$S^{(i)} = \prod_{t=0}^{24} (1 - q_{65+t,t}^{(i)}), \quad i = H, R,$$

where $q_{x,t}^{(i)}$ is the probability that an individual from population i dies in year t , given that the individual is alive and aged x at the beginning of year t . This survivor index is very similar to the one that is associated with the 25-year longevity bond that was announced by BNP Paribas and the European Investment Bank in 2004 (Blake et al., 2013).

We use the augmented common factor model proposed by Li and Lee (2005) to concurrently model the future mortality of all five populations. The model can be expressed as

$$\ln(m_{x,t}^{(i)}) = a_x^{(i)} + B_x K_t + b_x^{(i)} k_t^{(i)} + \epsilon_{x,t}^{(i)}, \quad i = H, R,$$

where $m_{x,t}^{(i)}$ denotes population i 's central death rate at age x and in year t , $a_x^{(i)}$ is a parameter measuring population i 's average level of mortality at age x , K_t is a time-varying index that is shared by all populations being modeled, $k_t^{(i)}$ is the time-varying index that is specific to population i , parameters B_x and $b_x^{(i)}$ respectively reflect the sensitivity to K_t and $k_t^{(i)}$ at age x , and $\epsilon_{x,t}^{(i)}$ is the error term.

Following Li and Lee, we estimate $a_x^{(i)}$ by setting it to the average of $\ln(m_{x,t}^{(i)})$ over the data sample period. To estimate B_x and K_t , we apply a first order singular value decomposition (SVD) to the matrix of $\sum_i w_{x,t}^{(i)} (\ln(m_{x,t}^{(i)}) - \hat{a}_x^{(i)})$, where $w_{x,t}^{(i)}$ represents population i 's number of exposures at age x and year t and the $\hat{\cdot}$ sign denotes an estimate. Another first order SVD is applied to the matrix of $\ln(m_{x,t}^{(i)}) - \hat{a}_x^{(i)} - \hat{B}_x \hat{K}_t$ to obtain estimates of parameters $b_x^{(i)}$ and $k_t^{(i)}$.

The evolution of K_t over time is modeled by a random walk with drift:

$$K_t = C + K_{t-1} + \xi_t,$$

where C is the drift term and $\{\xi_t\}$ is a sequence of i.i.d. normal random variables with zero mean and constant variance, whereas the evolution of $k_t^{(i)}$ over time is modeled by a first order autoregressive process:

$$k_t^{(i)} = \phi_0^{(i)} + \phi_1^{(i)} k_{t-1}^{(i)} + \zeta_t^{(i)},$$

where $\phi_0^{(i)}$ is a constant, $\phi_1^{(i)}$ is another constant whose absolute value is strictly less than one, and $\{\zeta_t^{(i)}\}$ is a sequence of i.i.d. normal random variables with zero mean and constant variance. The process for $k_t^{(i)}$ is mean-reverting, so that the projected mortality rates for different populations do not diverge indefinitely over time.

The model is fitted to historical data covering the age range of 60 to 89 and the sample period of 1960 to 2009. Most of the required data are obtained from the Human Mortality Database (2014). The only exception is the data for German males prior to 1991 (when the Berlin Wall fell), which are obtained from the LLMA.

Under the augmented common factor model, the probability distribution of $S^{(i)}$ cannot be written in closed-form; thus, the joint prediction regions cannot be derived analytically as was done by Chan et al. (2014). Instead, we obtain the joint prediction regions with the following numerical procedure:

1. Simulate 50,000 future values of $m_{x,t}^{(i)}$ from the estimated augmented common factor

Population	$h^{(R)}$
The US	1.3121
Germany	1.3804
The Netherlands	1.3718
England and Wales	1.3203

Table 1.1: The calculated values of $h^{(R)}$ for the four reference populations under consideration.

model. Using these simulated values and the approximation $q_{x,t}^{(i)} = 1 - \exp(-m_{x,t}^{(i)})$,⁴ calculate realizations of $I^{(H)}$ and $I^{(R)}$.

2. Using the realized values of $I^{(H)}$ and $I^{(R)}$, calculate the value of $h^{(R)}$ using the previously described linear regression methodology. The calculated values of $h^{(R)}$ for the four reference populations under consideration are displayed in Table 1.1.
3. Let $Y = (I^{(H)}, h^{(R)}I^{(R)})'$. For each simulated realization of Y , calculate its Mahalanobis distance to the best estimate as $Y'\hat{S}^{-1}Y$, where \hat{S} is the sample covariance matrix of Y . Note that the best estimate of Y is $E(Y) = (0, 0)'$. Geometrically speaking, the Mahalanobis distance may be viewed as the physical distance between the realization of Y and the origin, weighted by the standard deviations and covariance of $I^{(H)}$ and $h^{(R)}I^{(R)}$.⁵
4. Sort the 50,000 simulated realizations by their Mahalanobis distances to the best estimate. Choose the 50,000(1 - α) realizations with the shortest Mahalanobis distances.
5. Draw a convex hull to enclose the 50,000(1 - α) chosen realizations. In geometrical

⁴The approximation is exact if the force of mortality between two integer ages is constant.

⁵See Gnanadesikan and Kettenring (1972) for further information about Mahalanobis distances.

terms, the convex hull is the smallest convex set that contains the selected $50,000(1 - \alpha)$ pairs of $I^{(H)}$ and $h^{(R)}I^{(R)}$.

The convex hull drawn is a $100(1 - \alpha)\%$ joint prediction region for $I^{(H)}$ and $h^{(R)}I^{(R)}$, because by construction it contains a randomly selected pair of $I^{(H)}$ and $h^{(R)}I^{(R)}$ in the simulated sample with a probability of $1 - \alpha$. The use of a convex hull (the smallest convex set) prevents the joint prediction region from overstating the underlying uncertainty.

Figure 1.1 shows the graphical population basis risk metric when the reference population is English and Welsh males. The two dotted lines divide the diagram into four quadrants. The upper-right (lower-left) quadrant contains the outcomes when future mortality of both populations improves faster (slower) than expected, while the upper-left (lower-right) quadrant encompasses the outcomes when the mortality of Canadian males improves slower (faster) than expected and the mortality of English and Welsh males improves faster (slower) than expected. The dots in the diagram represent the 50,000 simulated pairs of $I^{(H)}$ and $h^{(R)}I^{(R)}$. These dots should align perfectly on the 45-degree line in the ideal case when there is no population basis risk. The region below the 45-degree line contains the under-hedging outcomes, while the region above contains the over-hedging outcomes. The vertical (or equivalently, horizontal) distance from an outcome to the 45-degree line indicates the extent of over- or under-hedging associated with that outcome. The likelihood of an outcome is visible from the colour shade of the region in which the outcome is located. Essentially, the darker the shading, the more likely the outcome.

The area spanned by the risk metric indicates the overall level of population basis risk. Therefore, one may determine the reference population that leads to the minimum amount

of basis risk by comparing the areas of the risk metrics for all available reference populations. Figure 1.2 displays the graphical risk metrics for all four reference populations under consideration. It is clear that the risk metric for U.S. males is smaller than the risk metrics for the other three available reference populations. Hence, for this hypothetical example, the hedger should choose to trade a derivative that is linked to U.S. male mortality.

1.4 Conclusion

In this chapter, we have proposed a graphical metric to intuitively communicate information about the level of population basis risk that an index-based longevity hedge is exposed to. The graphical risk metric is composed of a series of joint prediction regions of possible hedging outcomes, which are simulated from an assumed multi-population stochastic mortality model. Various aspects of population basis risk are reflected in the graphical risk metric. First, the area of a prediction region indicates the overall level of the population basis risk. Second, the shade of a prediction region reflects the likelihood of the hedging outcomes enclosed by the region. Third, the shape of the prediction region reveals how the hedger's liability is correlated with the survivor index to which the standardized hedging instrument is linked.

Compared to existing population basis risk metrics which are mostly numerical and only measure the overall risk level, the proposed metric is more informative in that it captures more aspects of population basis risk. Along with the existing numerical metrics, the proposed graphical metric may help potential hedgers better understand population basis risk and hence make their risk management decisions.

We have also illustrated the graphical population basis risk metric by a hypothetical example, in which the hedger's liability is associated with Canadian mortality while the available hedging instruments are linked respectively to the populations of the U.S., Germany, the Netherlands and England and Wales. Given the resulting joint prediction regions, one can easily tell that among the four reference populations, the U.S. is the most appropriate for the hypothetical hedger. We believe that as the market grows and standardized instruments linked to different reference populations become available, the proposed technique can assist hedgers with their choices of hedging instruments.

The graphical population basis risk metric depends on the assumed multi-population stochastic mortality model. Admittedly, the conclusions derived from the graphical metric may turn out to be different if another stochastic mortality model is assumed. It is warranted to explore in future work the robustness of the graphical risk metric relative to model choices. From a practical viewpoint, it would be useful to incorporate the proposed technique into existing stochastic mortality modeling software such as the LLMA's LifeMetrics. Such a development would allow potential hedgers to customize the graphical population basis risk metric on the basis of their own choices of mortality models and data sets.

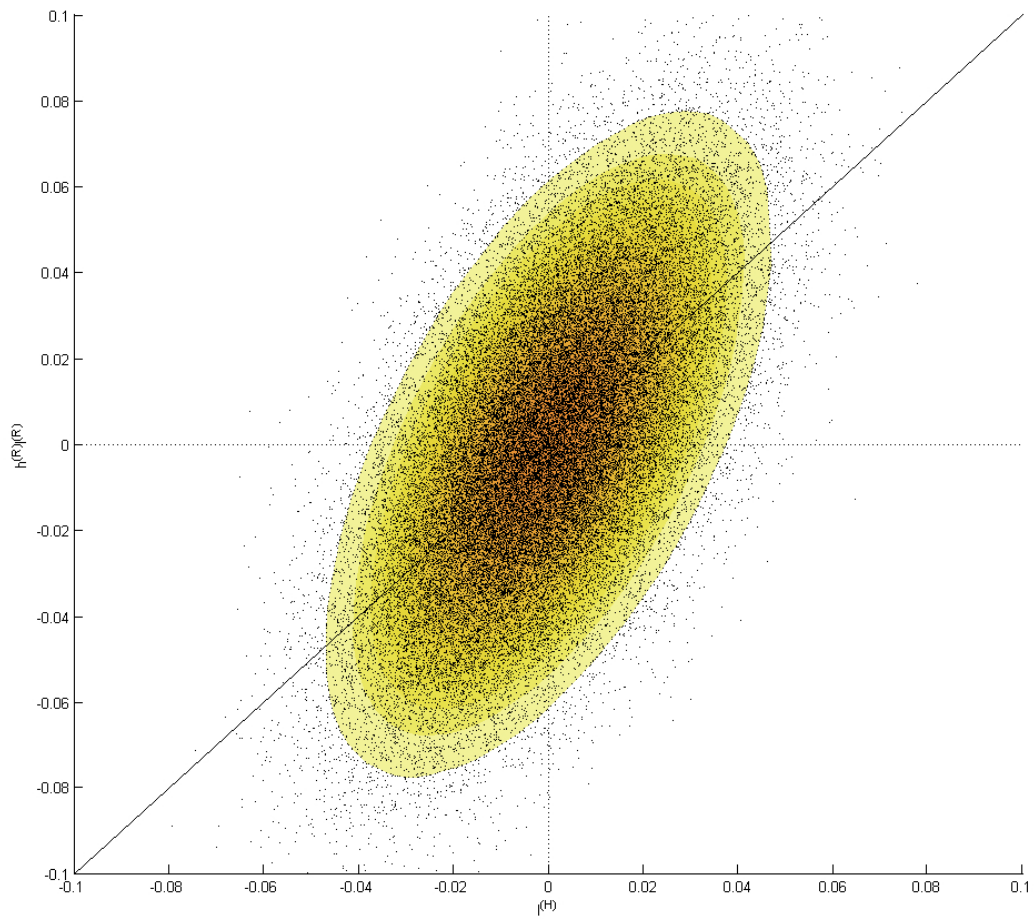


Figure 1.1: The graphical population basis risk metric for the situation when the hedger's population (H) is Canadian males and the derivative's reference population (R) is English and Welsh males. The dots represent the 50,000 simulated pairs of $I^{(H)}$ and $h^{(R)}I^{(R)}$.

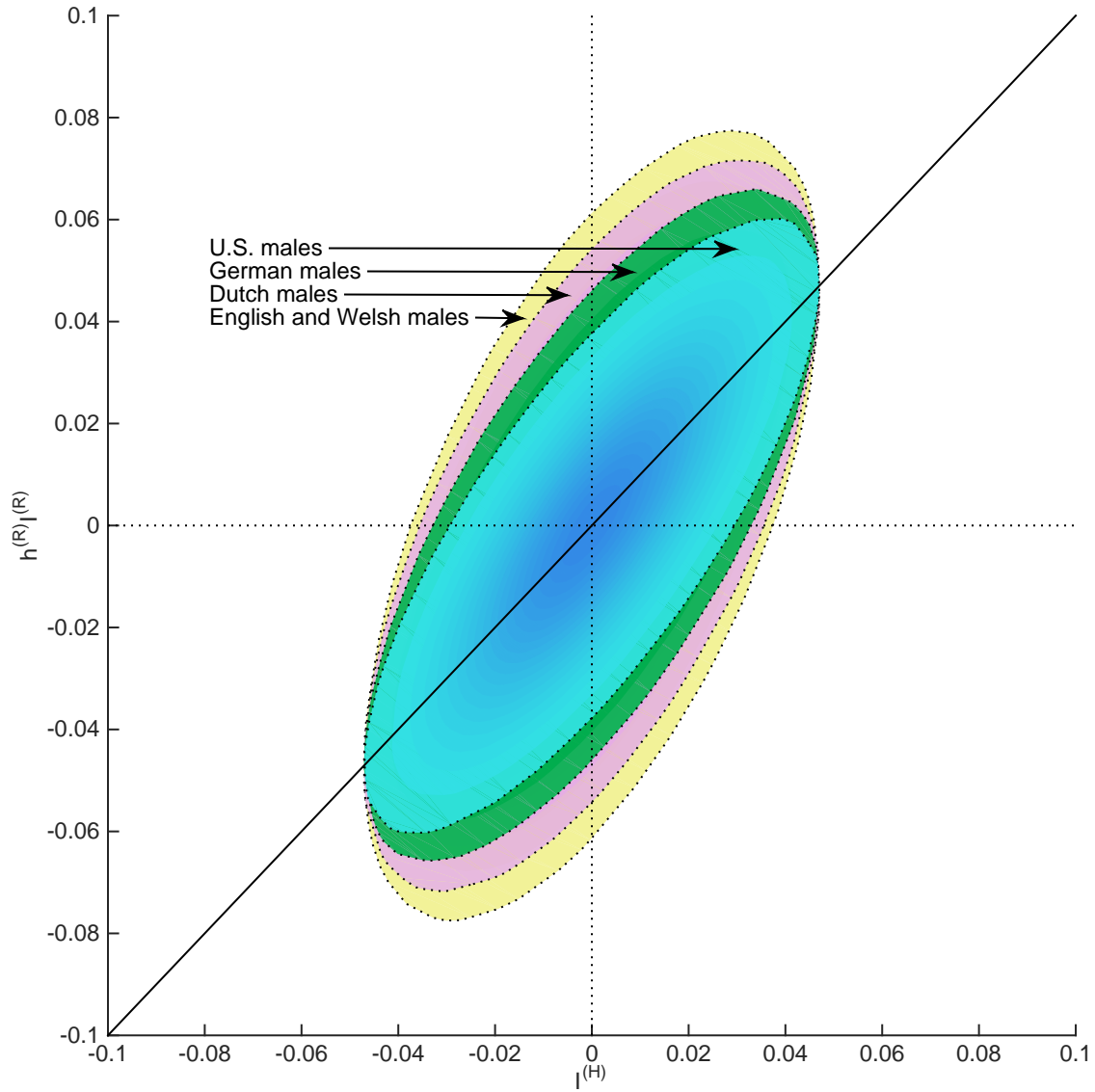


Figure 1.2: The graphical population basis risk metrics for the situations when the hedger's population (H) is Canadian males and the derivative's reference populations (R) are U.S. males, German males, Dutch males and English and Welsh males, respectively.

Chapter 2

Dynamic Longevity Hedging in the Presence of Population Basis Risk: A Feasibility Analysis from Technical and Economic Perspectives

2.1 Introduction

The market for longevity risk transfers started in about 10 years ago when the European Investment Bank and BNP Paribas experimented a 25-year longevity bond. Since then, the market has seen some significant developments, most notably in terms of the number and size of deals (Blake et al., 2014). However, relative to the size of the global longevity

risk exposure, the present longevity risk transfer market is still very small. A small market not only impedes longevity risk management, but also poses systemic concerns, because when longevity risk is shifted from the corporate sector to a limited number of (re)insurers, with global interconnections, there may be systemic consequences in the case of a failure of a key player (Basel Committee of Banking Supervision, 2013).

The underdevelopment of the longevity risk transfer market may be attributed to the marked imbalance between demand and supply. To date, most of the longevity risk transfers executed are insurance-based, typically in the form of pension buy-ins, pension buy-outs or bespoke longevity swaps. While the insurance industry has the scope and financial stability to assume longevity risk, it does not generate sufficient supply for acceptance of the risk because of its capacity constraints. Using the assets for pension plans, in excess of 31 trillion USD, as a proxy for demand and the assets of 2.6 trillion USD held by the global insurance industry to cover non-life risks as a proxy for supply, Graziani (2014) concluded that the demand for acceptance of longevity risk exceeds supply by a multiple of 10. Michealson and Mulholland (2014) also reached a similar conclusion by comparing the potential increase in pension liabilities due to unforeseen longevity improvement with the aggregate capital of the global insurance industry.

The demand and supply imbalance will only become worse if the reliance on the insurance industry to assume longevity risk continues. On one hand, the demand is expected to rise when pension plans in North America, where longevity risk was not widely recognized, begin to realize the materiality of the risk as they replace older mortality assumptions with the recently launched industry standards (the MP-2014 Scale for the US and the CPM-B Scale for Canada), which reflect the acceleration of mortality improvement happened over

the past two decades.¹ On the other hand, as Solvency II and its equivalence come into full effect, the insurance industry will be subject to more stringent capital requirements, which further compress the industry's ability to accept longevity risk exposures from pension plans.

The growth of the longevity risk transfer market therefore depends highly on the creation of supply, most likely by inviting participation from capital markets, which are capable of assuming a larger portion of the longevity risk exposures from pension plans around the world.² The longevity asset class offers capital market investors a risk premium, plus potential diversification benefits due to its very low correlation with literally every other asset class, including inflation, foreign exchange, commodities and equities (Ribeiro and di Pietro, 2009). However, drawing interest from such investors requires the longevity risk transfer market to package the risk as standardized products that are structured like typical capital market derivatives and linked to broad-based mortality indexes. The act of standardization is important in part because it fosters the development of liquidity, and in part because it removes the information asymmetry arising from the fact that hedgers (pension plans) have better knowledge about the mortality experience of their own portfolios.

Towards the goal of standardization, the market for longevity risk transfers has to overcome two technical challenges which discourage hedgers from using standardized hedging instruments. The first challenge is to find out how standardized instruments can be used to form a hedge that can eliminate a meaningful portion of the hedger's longevity risk exposure. Hedging strategies have to be developed so that hedgers know the type and

¹See the Society of Actuaries (2014) and the Canadian Institute of Actuaries (2014).

²According to Roxburgh (2011), the total value of the world's financial stock, comprising equity market capitalization and outstanding bonds and loans, is 212 trillion USD at the end of 2010.

notional amounts of hedging instruments they need to acquire. The second challenge is to understand and more importantly mitigate the residual risks that are left behind by a standardized, index-based longevity hedge. Of the residual risks the most significant constituent is population basis risk, which arises from the difference in future mortality improvements between the population associated with the hedger's own portfolio and the population(s) to which the standardized instruments are linked. However, as explained below, the research questions on longevity hedging strategies and population basis risk are still open.

A significant portion of the existing literature on longevity hedging strategies focuses on static hedging (Cairns, 2013; Cairns et al., 2006b, 2014; Coughlan et al., 2011; Dowd et al., 2011; Li and Hardy, 2011; Li and Luo, 2012). Broadly speaking, the static hedging strategies were derived by matching the sensitivities of the liability being hedged and portfolio of hedging instruments with respect to changes in the underlying mortality rates. Static hedging strategies are generally subject to the shortcoming of the need for long-dated hedging instruments. For example, in an illustrative static hedge for a 30-year pension liability, Li and Luo (2012) used five securities, of which the longest time-to-maturity is 25 years. Such long-dated securities do not seem appealing to capital market investors. A few researchers including Cairns (2011), Dahl (2004), Dahl and Møller (2006), Dahl et al. (2008) and Luciano et al. (2012) proposed dynamic longevity hedging strategies. Except the work of Cairns (2011), the existing dynamic longevity hedging strategies were developed from continuous-time models, which provide mathematical tractability but are not straightforward to implement in practice. Further, although some existing static hedging strategies include an adjustment for population basis risk (Dowd et al., 2011; Li and Hardy,

2011; Li and Luo, 2012), none of the aforementioned dynamic longevity hedging strategies takes population basis risk into account.

For the problem of population basis risk, researchers have recently contributed significantly to the development of multi-population stochastic mortality models (Ahmadi and Li, 2014; Cairns et al., 2011; Dowd et al., 2011; Hatzopoulos and Haberman, 2013; Jarner and Kryger, 2011; Li and Hardy, 2011; Li and Lee, 2005; Yang and Wang, 2013; Zhou et al., 2013, 2014). Such models can be regarded as a pre-requisite for understanding population basis risk, because they allow users to gauge the range of possible mortality differentials between two related populations, with biological reasonableness taken into consideration. Researchers have also introduced metrics for quantifying population basis risk, for example, reduction in expected shortfall (Ngai and Sherris, 2011), reduction in portfolio variance (Coughlan et al., 2011; Li and Hardy, 2011) and minimal required buffer (Stevens et al., 2011). However, to our knowledge, little attention has been paid to how population basis risk can be mitigated.

In this chapter, we attempt to address the limitations of the current literature by investigating how a dynamic, index-based longevity hedge can be performed when population basis risk is present and how the residual risks left behind by the hedge can be mitigated. Figure 2.1 provides a graphical illustration of the general framework on which this chapter is based. One part of the framework is a dynamic hedging strategy with which a pension plan can transfer the ‘trend risk’ (i.e., the risk surrounding the trend in longevity improvement) to capital markets, even if the securities available are linked to a broad-based mortality index. Another part of the framework is a specially designed reinsurance treaty, called a ‘customized surplus swap’, which transfers the residual risks to a reinsurer who

collectively manages the residual risks from the index-based longevity hedges of various pension plans.³

The dynamic hedging strategy we propose is obtained by generalizing the dynamic ‘delta’ hedging strategy of Cairns (2011) to incorporate the situation when the populations associated with the hedger’s portfolio and the hedging instruments are not the same. The generalization is derived on the basis of a multi-population stochastic mortality model, under which the mortality dynamics of different populations are non-trivially correlated. When implementing the proposed hedging strategy, the hedger needs to hold one only hedging instrument at a time and the hedging instrument can be shorter-dated. The former property helps the market to concentrate liquidity, while the latter property better meets the appetite of capital market investors. Adding further to the contribution of Cairns (2011) is a study of the robustness of the dynamic hedging strategy relative to different factors including model risk, small sample risk and the properties of the hedging instruments used.

The customized surplus swap we design eliminates all residual risks that are left behind by the dynamic longevity hedge. Therefore, the combination of a dynamic longevity hedge and customized surplus swap should produce the same hedge effectiveness as a typical bespoke longevity swap. Using real mortality data from 25 different populations, we demonstrate that the residual risks can potentially be diversified away when a reinsurer write customized surplus swaps with a range of hedgers. A reinsurer should thus have a

³A similar concept was mentioned by Cairns et al. (2008). In their set-up, hedgers transfer all their longevity risk exposures by writing bespoke longevity swaps with a special purposed vehicle (SPV), and the SPV in turn issues a standardized longevity bond which transfers the trend risk to the bondholders. The residual risks are borne by the SPV manager.

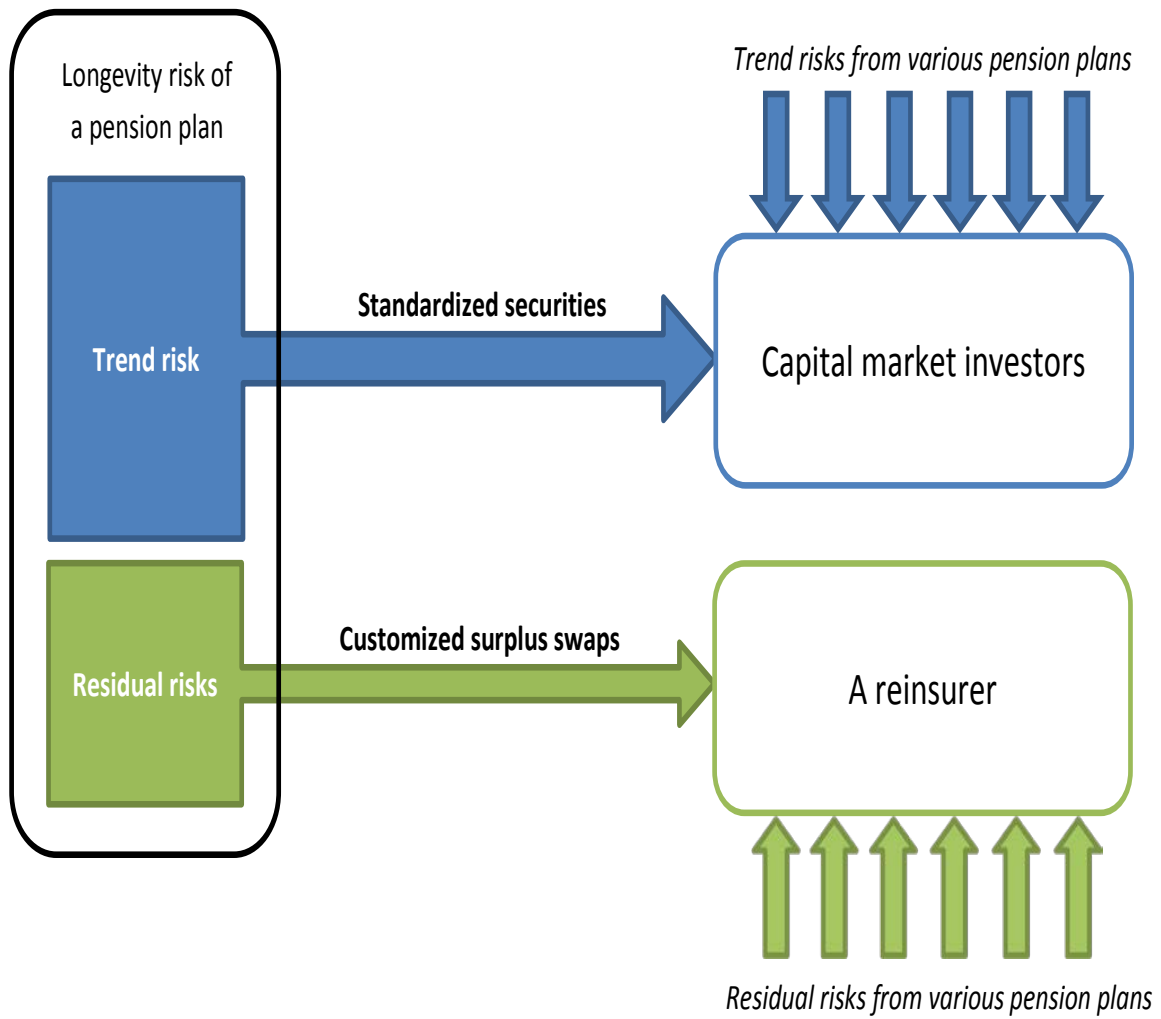


Figure 2.1: A graphical illustration of the general framework on which this chapter is based.

much larger capacity to write customized surplus swaps than contracts such as pension buy-outs which involve significant systematic risk. Overall, our proposed risk management framework is likely to be more economical than traditional longevity risk transfers that are entirely insurance-based, because in theory it is less costly to transfer the systematic trend risk through liquidly traded standardized securities than tailor-made (re)insurance contracts.

The rest of this chapter is organized as follows. Section 2.2 presents the technical details of the proposed dynamic hedging strategy. Section 2.3 illustrates the proposed dynamic hedging strategy and evaluates its robustness relative to various factors. Section 2.4 defines the proposed customized surplus swap and demonstrates the diversifiability of the residual risks. Finally, Section 2.5 concludes the chapter and discusses in more detail why the proposed risk management framework is likely to be more economical.

2.2 The Dynamic Longevity Hedging Strategy

2.2.1 The Assumed Model

The dynamic hedging strategy requires an assumed stochastic mortality model, from which quantities such as hedge ratios can be derived. In the single-population set-up of Cairns (2011), the original Cairns-Blake-Dowd model (a.k.a. Model M5) was assumed. In our multi-population generalization, we assume the augmented common factor (ACF) model proposed by Li and Lee (2005). The ACF model concurrently models the mortality dy-

namics of multiple, say P , populations as follows:

$$\ln(m_{x,t}^{(i)}) = a_x^{(i)} + B_x K_t + b_x^{(i)} k_t^{(i)} + \epsilon_{x,t}^{(i)}, \quad i = 1, \dots, P,$$

where $m_{x,t}^{(i)}$ represents population i 's central rate of death at age x and in year t , $a_x^{(i)}$ is a parameter indicating population i 's average level of mortality at age x , K_t is a time-varying index that is shared by all P populations, $k_t^{(i)}$ is a time-varying index that is specific to population i , parameters B_x and $b_x^{(i)}$ respectively reflect the sensitivity of $\ln(m_{x,t}^{(i)})$ to K_t and $k_t^{(i)}$, and $\epsilon_{x,t}^{(i)}$ is the error term that captures all remaining variations. Following Li and Lee (2005), we estimate the ACF model by the method of singular value decomposition.

The trend in K_t determines the evolution of mortality over time for all populations being modeled. As in the original Lee-Carter (Lee and Carter, 1992) model, K_t is assumed to follow a random walk with drift:

$$K_t = C + K_{t-1} + \xi_t,$$

where C is the drift term and $\{\xi_t\}$ is a sequence of i.i.d. normal random variables with zero mean and constant variance σ_K^2 .

Departures from the common time trend are captured by the population-specific index $k_t^{(i)}$, which is assumed to follow a first order autoregressive process:

$$k_t^{(i)} = \phi_0^{(i)} + \phi_1^{(i)} k_{t-1}^{(i)} + \zeta_t^{(i)},$$

where $\phi_0^{(i)}$ and $\phi_1^{(i)}$ are constants, and $\{\zeta_t^{(i)}\}$ is a sequence of i.i.d. normal random variables

with zero mean and constant variance $\sigma_{k,i}^2$. We require $|\phi_1^{(i)}| < 1$ so that the process for $k_t^{(i)}$ is mean-reverting. This property ensures that the resulting forecasts are coherent, which means the projected mortality rates for different populations do not diverge indefinitely over time. To incorporate any correlation that is not captured by the common trend K_t , we further assume that $\zeta_t^{(i)}$ and $\zeta_t^{(j)}$ for $i \neq j$ are constantly correlated, despite such correlations are not taken into account in the original ACF model.

2.2.2 The Set-up

We let

$$S_{x,t}^{(i)}(T) = \prod_{s=1}^T (1 - q_{x+s-1,t+s}^{(i)}) \quad (2.1)$$

be the *ex post* probability that an individual who is from population i and aged x at time t (the end of year t) would have survived to time $t + T$, where $q_{x,t}^{(i)}$ denotes the probability that an individual from population i dies between time $t - 1$ and t (during year t), provided that he/she has survived to age x at time $t - 1$. When computing $q_{x,t}^{(i)}$ from $m_{x,t}^{(i)}$ (on which the ACF model is based), we use the approximation $q_{x,t}^{(i)} \approx 1 - \exp(-m_{x,t}^{(i)})$.⁴ It is clear from the definitions that $S_{x,t}^{(i)}(T)$ is not known prior to time $t + T$, while $q_{x,t}^{(i)}$ is not known prior to time t .

Define by \mathcal{F}_t the information about the evolution of mortality up to and including time t . Due to the Markov property of the assumed stochastic processes, the value of $E(S_{x,u}^{(i)}(T)|\mathcal{F}_t)$ for $u \geq t$ depends only on the values of K_t and $k_t^{(i)}$ but not the values of K_v

⁴The approximation is exact if the force of mortality between two consecutive integer ages is constant.

and $k_v^{(i)}$ for $v < t$. Hence, we have

$$p_{x,u}^{(i)}(T, K_t, k_t^{(i)}) := \mathbb{E}(S_{x,u}^{(i)}(T) | K_t, k_t^{(i)}) = \mathbb{E}(S_{x,u}^{(i)}(T) | \mathcal{F}_t).$$

We call $p_{x,u}^{(i)}(T, K_t, k_t^{(i)})$ a spot survival probability when $u = t$ and a forward survival probability when $u > t$.

Let us suppose that the hedger intends to hedge the longevity risk associated with a pension plan for a single cohort of individuals, who are all from population H and aged x_0 at time 0. The plan pays each pensioner \$1 at the end of each year until death. It follows that the time- t value of the pension plan's future liabilities (per surviving pensioner at time t) can be expressed in terms of spot survival probabilities as

$$FL_t = \sum_{s=1}^{\infty} (1+r)^{-s} p_{x_0+t,t}^{(H)}(s, K_t, k_t^{(H)}),$$

where r is the interest rate for discounting purposes.

The hedging instruments are q-forwards that are associated with population R . A q-forward is a zero-coupon swap with its floating leg proportional to the realized death probability at a certain reference age during the year immediately prior to maturity and its fixed leg proportional to the corresponding pre-determined forward mortality rate. In this application, the hedger should participate in the q-forwards as the fixed-rate receiver, so that he/she will receive a net payment from the counterparty when mortality turns out to be lower than expected.

Consider a q-forward that is linked to reference population R and age x_f . Suppose

that the q-forward is issued at time t_0 and matures at time $t_0 + T^*$. The payoff from the q-forward depends on the realized value of $q_{x_f, t_0 + T^*}^{(R)}$. The corresponding forward mortality rate q^f is chosen so that no payment exchanges hands at inception (time t_0). It is assumed that $q^f = E(q_{x_f, t_0 + T^*}^{(R)} | \mathcal{F}_{t_0})$, which is equivalent to saying that no risk premium is given to the counterparty accepting the risk.⁵ At $t = t_0, \dots, t_0 + T^* - 1$, the value of the hedger's position of the q-forward (per \$1 notional) can be expressed as

$$\begin{aligned} Q_t(t_0) &= (1 + r)^{-(t_0 + T^* - t)} (q^f - E(q_{x_f, t_0 + T^*}^{(R)} | \mathcal{F}_t)) \\ &= (1 + r)^{-(t_0 + T^* - t)} (q^f - (1 - E(S_{x_f, t_0 + T^* - 1}^{(R)}(1) | \mathcal{F}_t))) \\ &= (1 + r)^{-(t_0 + T^* - t)} (q^f - (1 - p_{x_f, t_0 + T^* - 1}^{(R)}(1, K_t, k_t^{(R)}))). \end{aligned}$$

Under our pricing assumption, we have $Q_{t_0}(t_0) = 0$. Note that both FL_t and $Q_t(t_0)$ are related linearly to values of $p_{x,u}^{(i)}(T, K_t, k_t^{(i)})$, where $i = H, R$ and $u \geq t$.

The main idea behind the dynamic hedging strategy is that at each discrete time point t , the q-forward portfolio is adjusted so that FL_t and the adjusted q-forward portfolio have similar sensitivities to changes in the underlying common mortality index K_t . Hence, at each discrete time point t , we need to compute FL_t and $Q_t(t_0)$ and their partial derivatives with respect to K_t . However, because of the way in which $S_{x,t}^{(i)}(T)$ depends on K_u and $k_u^{(i)}$ for $u = t + 1, \dots, T$, the values of $p_{x,u}^{(i)}(T, K_t, k_t^{(i)})$ for $u \geq t$ (and thus FL_t and $Q_t(t_0)$) cannot be computed analytically. It follows that nested simulations are required, making

⁵Because the counterparty accepting longevity risk from the hedger deserves a risk premium, in practice q^f should be smaller than $E(q_{x_f, t_0 + T^*}^{(R)} | \mathcal{F}_{t_0})$, so that payoff to the counterparty is positive in expectation terms. However, because our focus for now is the technical aspects rather than the associated costs, we assume $q^f = E(q_{x_f, t_0 + T^*}^{(R)} | \mathcal{F}_{t_0})$ for simplicity.

the dynamic hedging framework strategy computationally challenging.

In more detail, let us assume that the hedging horizon is Y years and that the q-forward portfolio is adjusted annually. Suppose that N sample paths of future mortality (i.e., values of K_t , $k_t^{(H)}$ and $k_t^{(R)}$ for $t = 1, \dots, Y$) are used to evaluate the hedge's performance. For each of these N sample paths, we need to evaluate, at each time point t for $t = 1, \dots, Y$, FL_t and $Q_t(t_0)$ on the basis of the realized values of K_t , $k_t^{(H)}$ and $k_t^{(R)}$ in that particular sample path. If we calculate each FL_t and $Q_t(t_0)$ with M sample paths of mortality beyond time t , then in total we need to generate $N \times M \times Y$ sample paths. Because N and M are typically very large, say 10,000, the computational burden is huge.

To reduce computation burden, in the next subsection we derive formulas to approximate $p_{x,u}^{(i)}(T, K_t, k_t^{(i)})$ for $u \geq t$ so that the need for some of the simulations can be avoided. The accuracy of the approximation formulas is evaluated in Appendix A.

2.2.3 The Approximation Methods

The approximation formula for $p_{x,u}^{(i)}(T, K_t, k_t^{(i)})$ depends on whether $u = t$ or $u > t$.

Approximating $p_{x,u}^{(i)}(T, K_t, k_t^{(i)})$ when $u = t$

Following Cairns (2011), we approximate $p_{x,t}^{(i)}(T, K_t, k_t^{(i)})$ by applying a Taylor expansion to its probit transform, $f_{x,t}^{(i)}(T, K_t, k_t^{(i)}) := \Phi^{-1}(p_{x,t}^{(i)}(T, K_t, k_t^{(i)}))$, where Φ denotes the standard normal distribution function. The Taylor expansion is made around $\hat{K}_t = E(K_t|K_0)$ and

$\hat{k}_t^{(i)} = E(k_t^{(i)} | k_0^{(i)})$. We consider a second-order approximation, which means

$$\begin{aligned} f_{x,t}^{(i)}(T, K_t, k_t^{(i)}) &\approx D_{x,t,0}^{(i)}(T) + D_{x,t,1}^{(i)}(T)(K_t - \hat{K}_t) + D_{x,t,2}^{(i)}(T)(k_t^{(i)} - \hat{k}_t^{(i)}) \\ &\quad + \frac{1}{2}D_{x,t,3}^{(i)}(T)(K_t - \hat{K}_t)^2 + \frac{1}{2}D_{x,t,4}^{(i)}(T)(k_t^{(i)} - \hat{k}_t^{(i)})^2 \\ &\quad + D_{x,t,5}^{(i)}(T)(K_t - \hat{K}_t)(k_t^{(i)} - \hat{k}_t^{(i)}), \end{aligned}$$

where

$$\begin{aligned} D_{x,t,0}^{(i)}(T) &= f_{x,t}^{(i)}(T, \hat{K}_t, \hat{k}_t^{(i)}), & D_{x,t,1}^{(i)}(T) &= \left. \frac{\partial f_{x,t}^{(i)}(T, K_t, \hat{k}_t^{(i)})}{\partial K_t} \right|_{K_t = \hat{K}_t}, \\ D_{x,t,2}^{(i)}(T) &= \left. \frac{\partial f_{x,t}^{(i)}(T, \hat{K}_t, k_t^{(i)})}{\partial k_t^{(i)}} \right|_{k_t^{(i)} = \hat{k}_t^{(i)}}, & D_{x,t,3}^{(i)}(T) &= \left. \frac{\partial^2 f_{x,t}^{(i)}(T, K_t, \hat{k}_t^{(i)})}{\partial K_t^2} \right|_{K_t = \hat{K}_t}, \\ D_{x,t,4}^{(i)}(T) &= \left. \frac{\partial^2 f_{x,t}^{(i)}(T, \hat{K}_t, k_t^{(i)})}{\partial k_t^{2(i)}} \right|_{k_t^{(i)} = \hat{k}_t^{(i)}}, & D_{x,t,5}^{(i)}(T) &= \left. \frac{\partial^2 f_{x,t}^{(i)}(T, K_t, k_t^{(i)})}{\partial K_t \partial k_t^{(i)}} \right|_{K_t = \hat{K}_t, k_t^{(i)} = \hat{k}_t^{(i)}}. \end{aligned}$$

The values of $D_{x,t,j}^{(i)}(T)$ for $j = 1, \dots, 5$ are computed numerically as follows:

$$\begin{aligned} D_{x,t,1}^{(i)}(T) &\approx (f_{x,t}^{(i)}(T, \hat{K}_t + h, \hat{k}_t^{(i)}) - f_{x,t}^{(i)}(T, \hat{K}_t, \hat{k}_t^{(i)}))/h, \\ D_{x,t,2}^{(i)}(T) &\approx (f_{x,t}^{(i)}(T, \hat{K}_t, \hat{k}_t^{(i)} + h) - f_{x,t}^{(i)}(T, \hat{K}_t, \hat{k}_t^{(i)}))/h, \\ D_{x,t,3}^{(i)}(T) &\approx (f_{x,t}^{(i)}(T, \hat{K}_t + h, \hat{k}_t^{(i)}) + f_{x,t}^{(i)}(T, \hat{K}_t - h, \hat{k}_t^{(i)}) - 2f_{x,t}^{(i)}(T, \hat{K}_t, \hat{k}_t^{(i)}))/h^2, \\ D_{x,t,4}^{(i)}(T) &\approx (f_{x,t}^{(i)}(T, \hat{K}_t, \hat{k}_t^{(i)} + h) + f_{x,t}^{(i)}(T, \hat{K}_t, \hat{k}_t^{(i)} - h) - 2f_{x,t}^{(i)}(T, \hat{K}_t, \hat{k}_t^{(i)}))/h^2, \\ D_{x,t,5}^{(i)}(T) &\approx (f_{x,t}^{(i)}(T, \hat{K}_t + h, \hat{k}_t^{(i)} + h) + f_{x,t}^{(i)}(T, \hat{K}_t - h, \hat{k}_t^{(i)} - h) \\ &\quad - f_{x,t}^{(i)}(T, \hat{K}_t + h, \hat{k}_t^{(i)} - h) - f_{x,t}^{(i)}(T, \hat{K}_t - h, \hat{k}_t^{(i)} + h))/4h^2, \end{aligned}$$

where h is an arbitrarily small positive value.

To calculate the above partial derivatives for a fixed t , we require nine sets of M sample mortality paths, which are respectively based on nine different sets of starting values, including $(K_t = \hat{K}_t, k_t^{(i)} = \hat{k}_t^{(i)})$, $(K_t = \hat{K}_t + h, k_t^{(i)} = \hat{k}_t^{(i)})$, $(K_t = \hat{K}_t, k_t^{(i)} = \hat{k}_t^{(i)} + h)$ and so on. For a hedging horizon of Y time steps, the number of sample paths required to generate the partial derivatives is $9 \times M \times Y$.

Suppose again that N mortality scenarios are used to evaluate the hedge's performance. Because the partial derivatives are independent of these N mortality scenarios, the total number of sample paths we need to generate is $N + 9 \times M \times Y$, which is significantly smaller than $N \times M \times Y$ when N and M are large.

Approximating $p_{x,u}^{(i)}(T, K_t, k_t^{(i)})$ when $u > t$

Using a first-order approximation, it can be shown that

$$p_{x,u}^{(i)}(T, K_t, k_t^{(i)}) \approx \Phi \left(\frac{-\mathbb{E}(V_u^{(i)} | \mathcal{F}_t)}{\sqrt{\text{Var}(V_u^{(i)} | \mathcal{F}_t)}} \right),$$

where

$$\mathbb{E}(V_u^{(i)} | \mathcal{F}_t) = -D_{x,u,0}^{(i)}(T) - D_{x,u,1}^{(i)}(T)(\mathbb{E}(K_u | \mathcal{F}_t) - \hat{K}_u) - D_{x,u,2}^{(i)}(T)(\mathbb{E}(k_u^{(i)} | \mathcal{F}_t) - \hat{k}_u^{(i)}),$$

$$\text{Var}(V_u^{(i)} | \mathcal{F}_t) = 1 + (D_{x,u,1}^{(i)}(T))^2 \text{Var}(K_u | \mathcal{F}_t) + (D_{x,u,2}^{(i)}(T))^2 \text{Var}(k_u^{(i)} | \mathcal{F}_t),$$

$$\mathbb{E}(K_u | \mathcal{F}_t) - \hat{K}_u = K_t - K_0 - Ct,$$

$$\mathbb{E}(k_u^{(i)} | \mathcal{F}_t) - \hat{k}_u = (\phi_1^{(i)})^u ((\phi_1^{(i)})^{-t} k_t^{(i)} - k_0^{(i)}) + \frac{(\phi_1^{(i)})^u (1 - (\phi_1^{(i)})^{-t})}{1 - \phi_1^{(i)}} \phi_0^{(i)},$$

$\text{Var}(K_u|\mathcal{F}_t) = \sigma_K^2(u-t)$ and $\text{Var}(k_u^{(i)}|\mathcal{F}_t) = \frac{1-(\phi_1^{(i)})^{2(u-t)}}{1-(\phi_1^{(i)})^2} \sigma_{k,i}^2$. A proof of the above approximation formula is provided in Appendix B.

2.2.4 Deriving Hedge Ratios

Our goal is to ensure that at each discrete time point t , the q-forward portfolio and the pension plan's future liabilities have similar sensitivities to changes in the underlying common mortality index K_t . To achieve this goal, the hedge ratio h_t (i.e., the notional amount of the q-forward) at time t is chosen in such a way that

$$\frac{\partial FL_t}{\partial K_t} = h_t \frac{\partial Q_t(t_0)}{\partial K_t}.$$

Because we match the first derivatives only, only one q-forward contract is needed at each t . For the same reason, our hedge may be considered as a 'delta' hedge. In principle, one may create, for example, a 'gamma' hedge by matching also the second order derivatives. The next chapter explores 'delta' and 'gamma' hedges in a static set-up.

The partial derivative of FL_t with respect to K_t is computed as follows:

$$\begin{aligned} \frac{\partial FL_t}{\partial K_t} &= \sum_{s=1}^{\infty} (1+r)^{-s} \frac{\partial p_{x_0+t,t}^{(H)}(s, K_t, k_t^{(H)})}{\partial K_t} \\ &= \sum_{s=1}^{\infty} (1+r)^{-s} \frac{\partial \Phi(f_{x_0+t,t}^{(H)}(s, K_t, k_t^{(H)}))}{\partial K_t} \\ &\approx \sum_{s=1}^{\infty} (1+r)^{-s} D_{x_0+t,t,1}^{(H)}(s) \phi(f_{x_0+t,t}^{(H)}(s, K_t, k_t^{(H)})), \end{aligned}$$

where ϕ represents the probability density function for a standard normal random variable.

The partial derivative of $Q_t(t_0)$ with respect to K_t depends on the value of t relative to the q-forward's maturity date $t_0 + T^*$. If $t = t_0 + T^* - 1$,

$$\frac{\partial Q_t(t_0)}{\partial K_t} = (1+r)^{-1} \frac{\partial p_{x_f,t}^{(R)}(1, K_t, k_t^{(R)})}{\partial K_t} \approx (1+r)^{-1} D_{x_f,t,1}^{(R)}(1) \phi(f_{x_f,t}^{(R)}(1, K_t, k_t^{(R)})).$$

If $t = t_0, \dots, t_0 + T^* - 2$,

$$\begin{aligned} \frac{\partial Q_t(t_0)}{\partial K_t} &= (1+r)^{-(t_0+T^*-t)} \frac{\partial p_{x_f,t_0+T^*-1}^{(R)}(1, K_t, k_t^{(R)})}{\partial K_t} \\ &\approx (1+r)^{-(t_0+T^*-t)} \frac{\partial}{\partial K_t} \Phi \left(\frac{-E(V_{t_0+T^*-1}^{(R)} | \mathcal{F}_t)}{\sqrt{\text{Var}(V_{t_0+T^*-1}^{(R)} | \mathcal{F}_t)}} \right) \\ &= (1+r)^{-(t_0+T^*-t)} \phi \left(\frac{-E(V_{t_0+T^*-1}^{(R)} | \mathcal{F}_t)}{\sqrt{\text{Var}(V_{t_0+T^*-1}^{(R)} | \mathcal{F}_t)}} \right) \frac{-D_{x_f,t_0+T^*-1,1}^{(R)}(1)}{\sqrt{\text{Var}(V_{t_0+T^*-1}^{(R)} | \mathcal{F}_t)}}. \end{aligned}$$

2.2.5 Evaluating the Hedge

As previously mentioned, N mortality scenarios are simulated to evaluate the effectiveness of the dynamic hedge.

Define by PL_t the time-0 value of all pension liabilities, given the information up to

and including time t ; that is,

$$\begin{aligned}
PL_t &= \mathbb{E} \left(\sum_{s=1}^{\infty} (1+r)^{-s} S_{x_0,0}^{(H)}(s) \middle| \mathcal{F}_t \right) \\
&= \begin{cases} FL_0, & t = 0 \\ \sum_{s=1}^t (1+r)^{-s} S_{x_0,0}^{(H)}(s) + (1+r)^{-t} S_{x_0,0}^{(H)}(t) FL_t, & t > 0. \end{cases} \quad (2.2)
\end{aligned}$$

The value of PL_0 is non-random, as it is simply a function of K_0 and $k_0^{(H)}$ whose values are fixed. For $t > 0$, the values of PL_t are different under different simulated mortality scenarios. In particular, the values of $S_{x_0,0}^{(H)}(s)$ for $s = 1, \dots, t$ depend on the realized values of K_s and $k_s^{(H)}$ for $s = 1, \dots, t$, whereas the value of FL_t depends on the realized values of K_t and $k_t^{(H)}$.

It is assumed that at each time point t , the hedger writes a new q-forward contract (i.e., a q-forward with inception date $t_0 = t$) with a notional amount of h_t . The value of this position is $h_t Q_t(t) = 0$ at time t and becomes

$$\begin{aligned}
h_t Q_{t+1}(t) &= h_t (1+r)^{-(T^*-1)} (q^f - \mathbb{E}(q_{x_f, t+T^*}^{(R)} | \mathcal{F}_{t+1})) \\
&= h_t (1+r)^{-(T^*-1)} (\mathbb{E}(q_{x_f, t+T^*}^{(R)} | \mathcal{F}_t) - \mathbb{E}(q_{x_f, t+T^*}^{(R)} | \mathcal{F}_{t+1})) \\
&= h_t (1+r)^{-(T^*-1)} (p_{x_f, t+T^*-1}^{(R)}(1, K_{t+1}, k_{t+1}^{(R)}) - p_{x_f, t+T^*-1}^{(R)}(1, K_t, k_t^{(R)}))
\end{aligned}$$

at time $t+1$.⁶ At time $t+1$, the position written at time t is closed out, and another new q-forward contract is written. The process repeats until the end of the hedging horizon Y is reached. For simplicity, we assume that all q-forwards used over the hedging horizon

⁶The second step is due to our pricing assumption.

have the same maturity T^* and reference age x_f .

Let PA_t be the time-0 value of the assets backing the pension plan at time t . We assume that $PA_0 = PL_0$. For $t = 1, \dots, Y$, we have

$$PA_t = PA_{t-1} + (1+r)^{-t} h_{t-1} Q_t(t-1).$$

If PA_t is very close to PL_t for $t = 1, \dots, Y$, then the dynamic hedge can be said as successful. The potential deviation between PA_t and PL_t is the residual risk that is not mitigated by the hedge. Using this reasoning, we measure hedge effectiveness by the following metric:

$$HE_t = 1 - \frac{\text{Var}(PA_t - PL_t | \mathcal{F}_0)}{\text{Var}(PL_t | \mathcal{F}_0)}.$$

A value of HE_t that is close to one indicates the hedge is effective. Similar metrics have been used by Cairns (2011, 2013), Cairns et al. (2014), Coughlan et al. (2011) and Li and Hardy (2011).

2.3 Analyzing the Dynamic Longevity Hedge

2.3.1 Assumptions

The following assumptions are used in the baseline calculations.

1. The hedger wishes to hedge the pension liabilities that are payable to a single cohort of individuals, who are all aged $x_0 = 60$ at time 0. The mortality experience of these

individuals is identical to that of the UK male insured lives.

2. The pension plan pays each individual \$1 at the end of each year until death or age 90, whichever the earliest. ⁷
3. The hedging horizon is $Y = 30$ years (i.e., the hedge stops when the liabilities have completely run off).
4. The q-forwards used are linked to England and Wales (EW) male population. They all have a time-to-maturity (from inception) of $T^* = 10$ years and a reference age of $x_f = 75$.
5. The market for the q-forwards is liquid and no transaction cost is required.
6. The interest rate for all durations is $r = 4\%$ per annum. The interest rate remains constant over time.
7. The hedger can invest or borrow at an interest rate of $r = 4\%$ per annum.
8. The values of $D_{x,t,j}^{(i)}(T)$ for $i = H, R$ and $j = 0, \dots, 5$ are computed from an ACF model that is estimated to the data from the populations of EW males and UK male insured lives over the period of 1966 to 2005 and the age range of 60 to 89. ⁸
9. To match the end point of the data sample period, time 0 is set to the end of year 2005.

⁷We assume that no pension is payable beyond age 90, because the upper limit of the age range to which the ACF model is fitted is 89. This assumption may be relaxed if one assumes a parametric curve to extrapolate death probabilities beyond age 89.

⁸The data for EW males are provided by the Human Mortality Database (2014), while the data for UK male insured lives are obtained from the Institute and Faculty of Actuaries by a written request.

10. The evaluation of hedge effectiveness is based on $N = 10,000$ mortality scenarios that are generated from the model described in Assumption (8).
11. There is no small sample risk.

2.3.2 Baseline Results

Let us first study the calculation of hedge ratios at different time points. The fan charts in Figure 2.2 show the distributions of $\frac{\partial FL_t}{\partial K_t} | \mathcal{F}_0$, $\frac{\partial Q_t(t)}{\partial K_t} | \mathcal{F}_0$ and $h_t | \mathcal{F}_0$ for $t = 0, \dots, 29$.⁹

The values of $\frac{\partial FL_t}{\partial K_t}$ for $t = 0, \dots, 29$ are negative, because the value of future liabilities reduces when K_t is larger (i.e., mortality becomes higher). As the liabilities run off, the magnitude of $\frac{\partial FL_t}{\partial K_t}$ reduces gradually to zero. The uncertainty surrounding $\frac{\partial FL_t}{\partial K_t} | \mathcal{F}_0$ increases with time initially but then reduces gradually to zero. The initial increase in uncertainty is because $\frac{\partial FL_t}{\partial K_t}$ is a function of K_t whose randomness (given \mathcal{F}_0) increases with time, while the reduction afterwards is because the liabilities run off.

The values of $\frac{\partial Q_t(t)}{\partial K_t}$ for $t = 0, \dots, 29$ are also negative, because from the viewpoint of the hedger (who participates in the q-forward as a fixed rate receiver), the value of the q-forward portfolio is smaller if the floating rate goes up, which happens when K_t is larger. The value of $\frac{\partial Q_t(t)}{\partial K_t}$ approaches (slowly) to zero, because the value of $q_{75,t+10}^{(R)}$ on which $Q_t(t)$ depends tends slowly to zero as mortality improves over time. The uncertainty surrounding $\frac{\partial Q_t(t)}{\partial K_t} | \mathcal{F}_0$ increases with t , because $\frac{\partial Q_t(t)}{\partial K_t}$ is a function of K_t which is subject to increasing randomness over time. The slow reduction in $q_{75,t+10}^{(R)}$ may have an impact on

⁹Each fan chart shows the central 10% prediction interval with the heaviest shading, surrounded by the 20%, 30%, ..., 90% prediction intervals with progressively lighter shading.

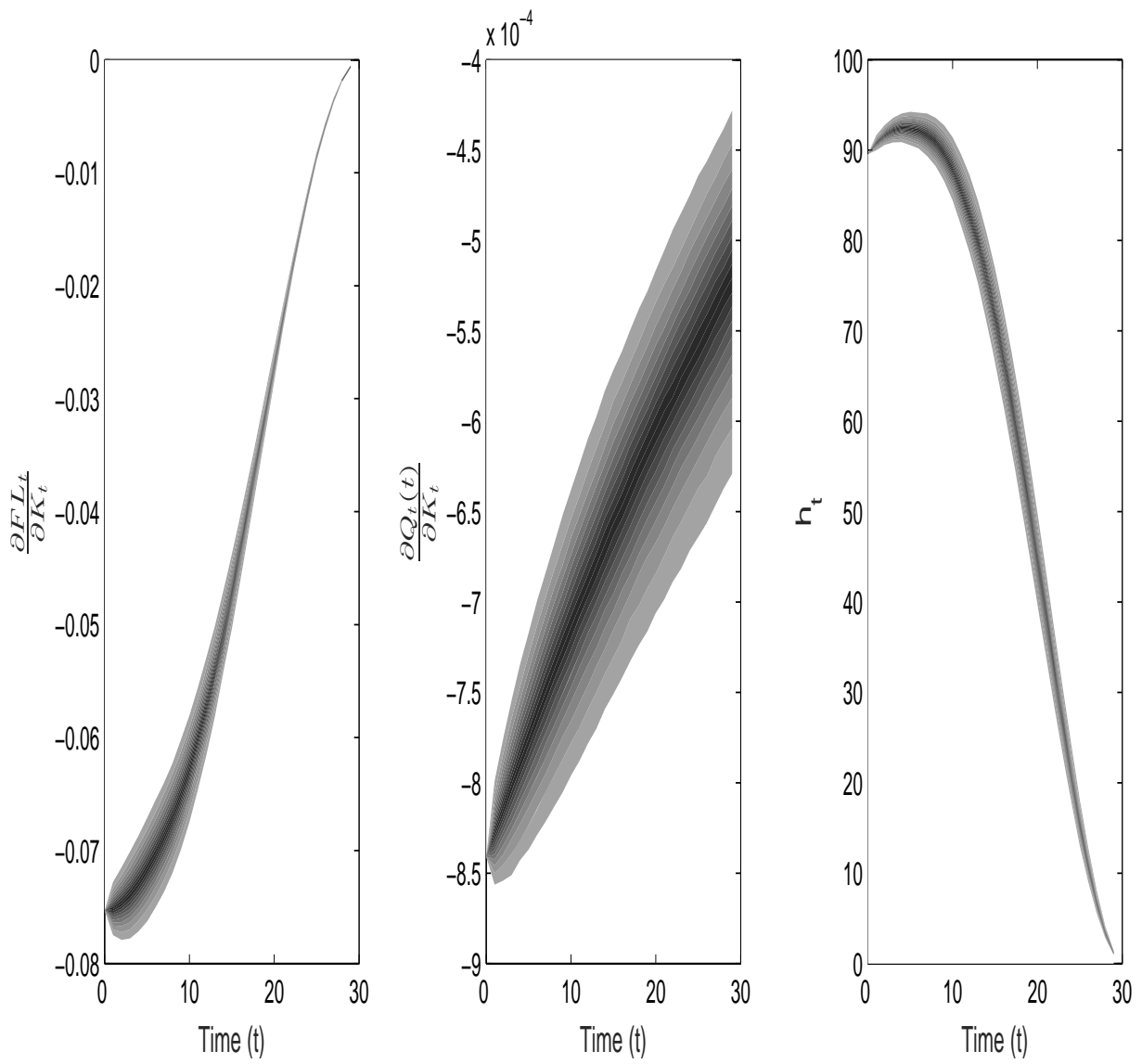


Figure 2.2: Fan charts showing the distributions of $\frac{\partial FL_t}{\partial K_t}|\mathcal{F}_0$, $\frac{\partial Q_t(t)}{\partial K_t}|\mathcal{F}_0$ and $h_t|\mathcal{F}_0$.

the uncertainty but is negligible.

The value of h_t , which is the ratio of $\frac{\partial FL_t}{\partial K_t}$ to $\frac{\partial Q_t(t)}{\partial K_t}$, increases first but then decreases. This pattern may be explained by the gradients of the trends in $\frac{\partial FL_t}{\partial K_t}$ and $\frac{\partial Q_t(t)}{\partial K_t}$. In particular, the initial increase in h_t is because the magnitude of $\frac{\partial Q_t(t)}{\partial K_t}$ reduces much more rapidly than that of $\frac{\partial FL_t}{\partial K_t}$. As expected, the value of h_t reduces to zero at $t = 30$ when the liabilities run off completely.

We now move on to studying the hedged and unhedged liabilities over time. The gray (larger) fan chart in Figure 2.3 depicts the distributions of $(PL_t - PL_0)|\mathcal{F}_0$ (or equivalently $PL_t|\mathcal{F}_0$) for $t = 0, \dots, 30$. When there is no longevity hedge, the time-0 value of the assets backing the pension plan is always FL_0 , because we assume $PA_0 = PL_0 = FL_0$. Hence, $PL_t - PL_0$ can be regarded as the shortfall in assets in the absence of a longevity hedge. The uncertainty surrounding $PL_t|\mathcal{F}_0$ increases with t , but becomes stable as $t \rightarrow 30$. The increase in uncertainty is because in comparison to PL_{t-1} , PL_t depends on two additional random variables, K_t and $k_t^{(H)}$. The reduction in the rate of increase can be explained by the following equation:

$$PL_t - PL_{t-1} = (1+r)^{-t}(S_{60,0}^{(H)}(t) + S_{60,0}^{(H)}(t)FL_t - (1+r)S_{60,0}^{(H)}(t-1)FL_{t-1}),$$

$t = 2, \dots, 30$, which is obtained straightforwardly from equation (2.2). As $t \rightarrow 30$, $S_{60,0}^{(H)}(t)$, FL_t , $(1+r)^{-t}$ and hence $PL_t - PL_{t-1}$ tend to zero. The sample paths of PL_t therefore become flat gradually, which implies the distribution of $PL_t|\mathcal{F}_0$ becomes increasingly invariant with time.

The green (smaller) fan chart in Figure 2.3 shows the distributions of $(PL_t - PA_t)|\mathcal{F}_0$

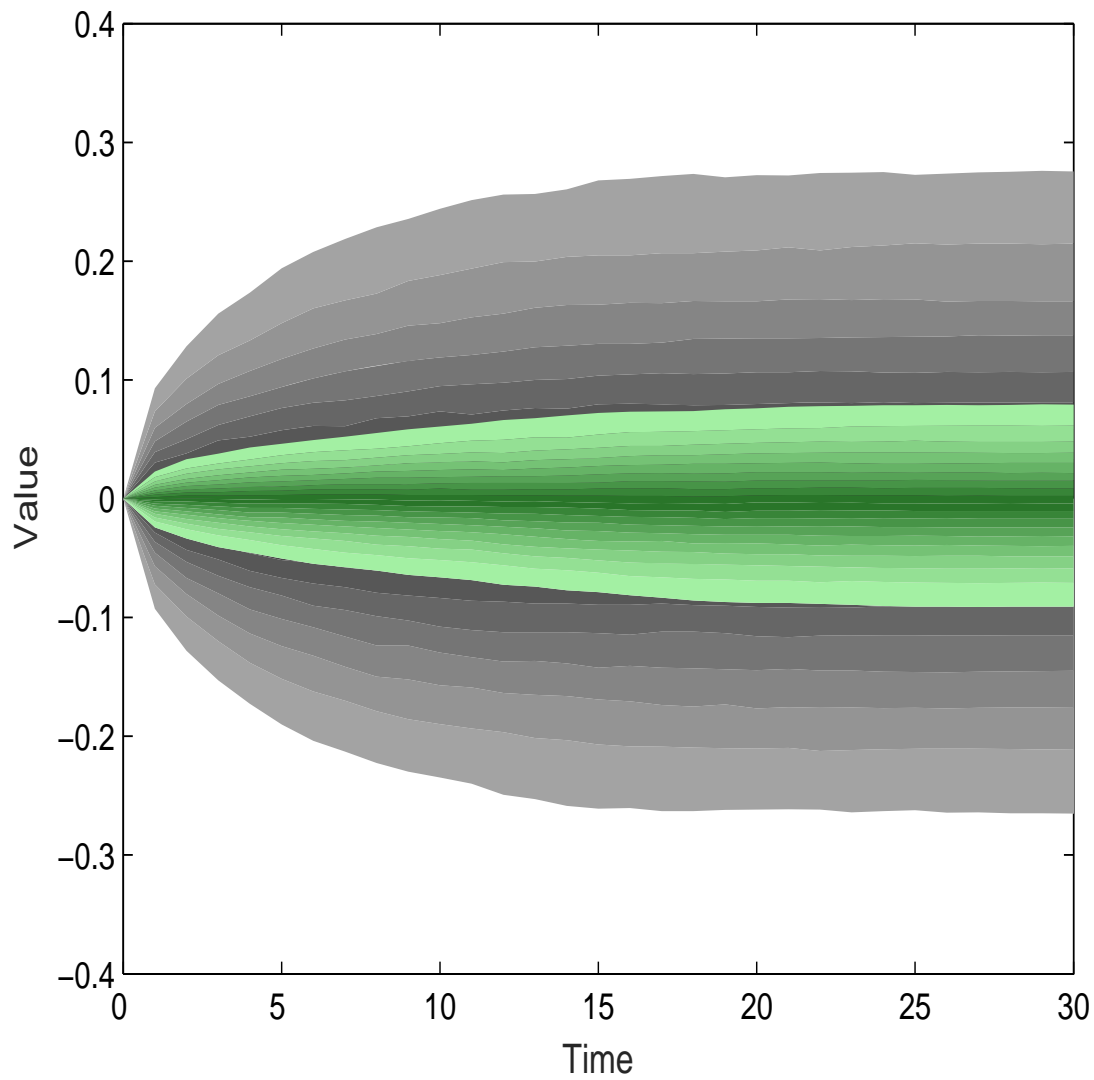


Figure 2.3: Fan charts showing the distributions of $(PL_t - PL_0)|\mathcal{F}_0$ (in gray) and $(PL_t - PA_t)|\mathcal{F}_0$ (in green) when population basis risk is present (i.e. the q-forwards are linked to EW male population).

for $t = 0, \dots, 30$. We can regard $PL_t - PA_t$ as the shortfall in assets when a dynamic longevity hedge is in place. Over the entire hedging horizon, $(PL_t - PA_t)|\mathcal{F}_0$ is significantly less dispersed than $(PL_t - PL_0)|\mathcal{F}_0$, indicating that the longevity hedge is effective. The hedge effectiveness can be seen more clearly from the red line in Figure 2.4, which shows that the value of HE_t is consistently larger than 90%.

To assess the extent of population basis risk, we repeat the calculations by assuming, hypothetically, that q-forwards linked to the population of UK male insured lives are available and used. The hedging results are shown in Figure 2.5.¹⁰ The degree of population basis risk can be observed from the difference in the widths of the green fan charts in Figures 2.3 and 2.5. It can also be assessed by comparing the values of HE_t when population basis risk is present and hypothetically absent in Figure 2.4.

2.3.3 Robustness

In this subsection, we test the robustness of the hedge effectiveness relative to model risk, small sample risk, the q-forwards' reference age and the q-forwards' time-to-maturity.

Robustness Relative to Model Risk

We now study how hedge effectiveness may change when the actual underlying model is not the ACF model on which valuation and calculation of hedge ratios are based. To

¹⁰When modeling only one population, the ACF model degenerates to the original Lee-Carter Model. The results shown in Figure 2.5 are therefore derived from the original Lee-Carter model which is fitted to data from UK male insured lives only. Because different models are used, the gray fan charts in Figures 2.3 and 2.5 are slightly different.

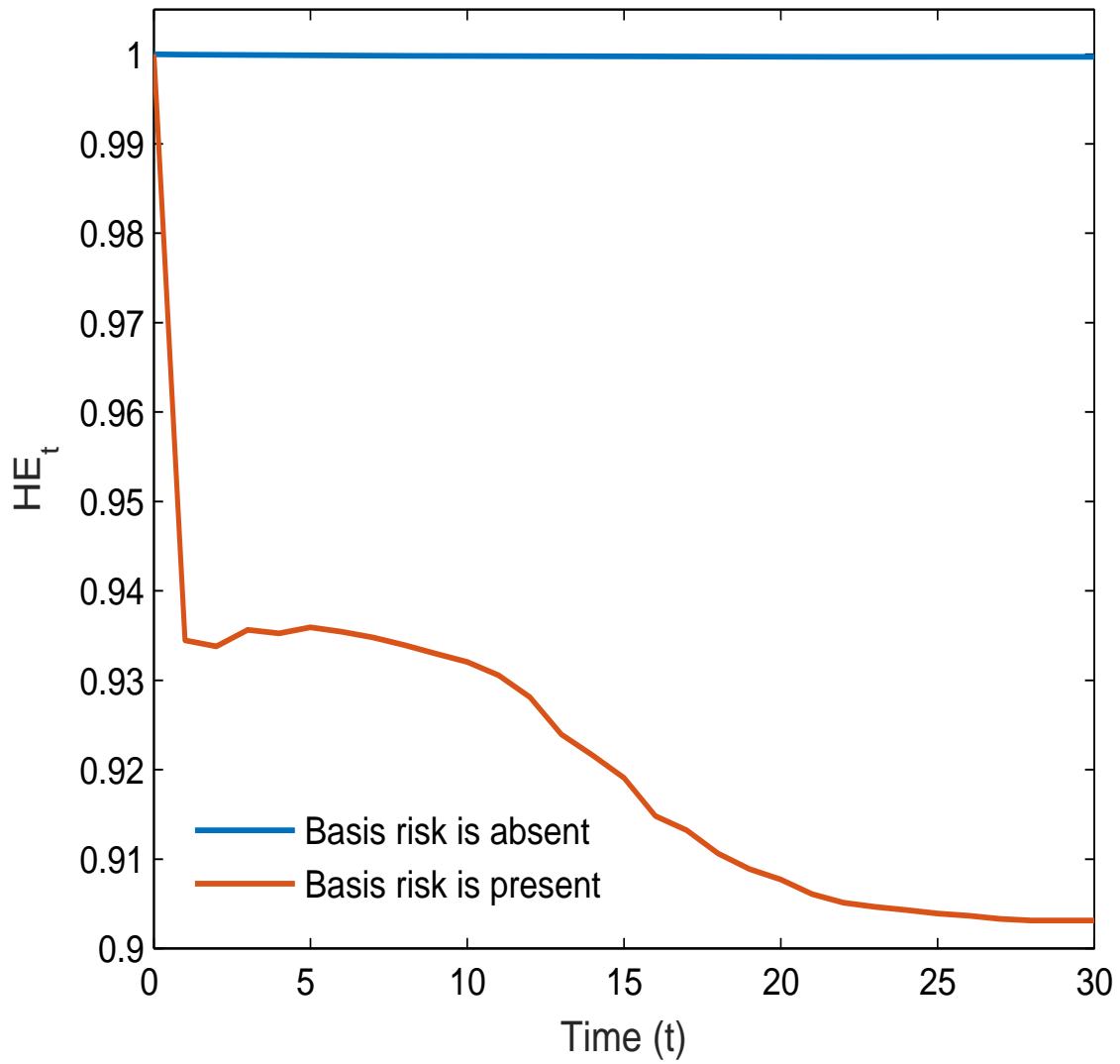


Figure 2.4: The values of HE_t for $t = 0, \dots, 30$ when population basis risk is present (the red line) and hypothetically absent (the blue line).

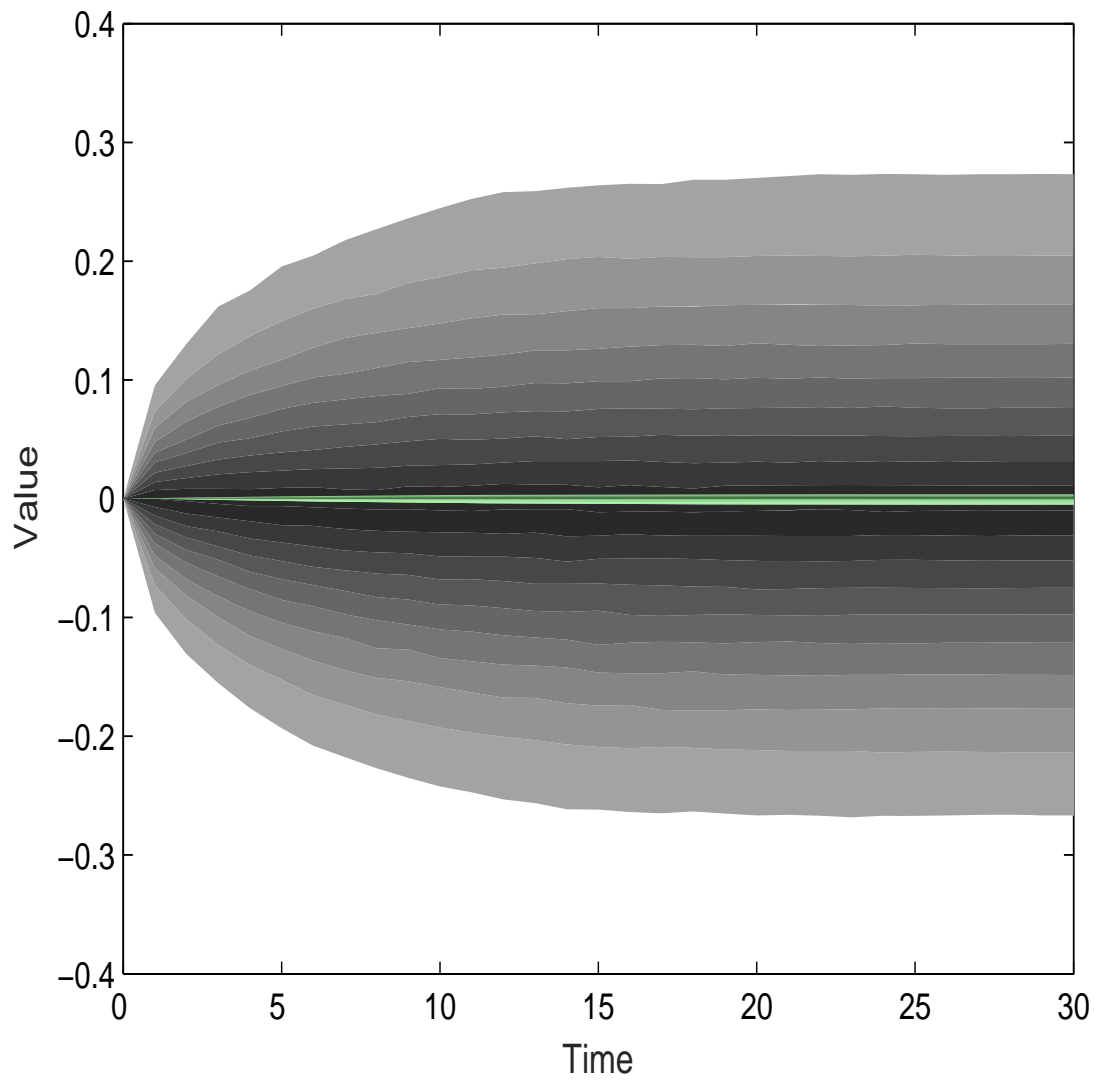


Figure 2.5: Fan charts showing the distributions of $(PL_t - PL_0)|\mathcal{F}_0$ (in gray) and $(PL_t - PA_t)|\mathcal{F}_0$ (in green) when population basis risk is absent (i.e. the q-forwards are linked to the population of UK male insured lives).

mimic this situation, we use an alternative stochastic model to generate the N mortality scenarios for assessing hedge effectiveness, while the ACF model is still used for valuation and calculation of hedge ratios. The following two alternative models are considered.

- An asymmetric multi-population Lee-Carter model (M-LC)

Originally proposed by Cairns et al. (2011), the M-LC model has the following structure:

$$\ln(m_{x,t}^{(i)}) = \alpha_x^{(i)} + \beta_x \kappa_t^{(i)} + e_{x,t}^{(i)}, \quad i = 1, \dots, P,$$

where $\alpha_x^{(i)}$ and β_x are age-specific parameters, $\kappa_t^{(i)}$ is a time-varying parameter and $e_{x,t}^{(i)}$ is the error term. The model is considered as asymmetric, because one population being modeled (say population i_d) is assumed to be dominant, driving the mortality dynamics of the other populations. The evolution of $\kappa_t^{(i_d)}$ over time is modeled by a random walk with drift, while the differential $\kappa_t^{(i_d)} - \kappa_t^{(i)}$ for $i \neq i_d$ is modeled by a first order autoregressive process. These processes ensure the resulting forecast is coherent.

In our illustration, we estimate the M-LC model to data from EW males and UK male insured lives, with the assumption that the dominant population is EW males. The method of singular value decomposition is used to estimate the model.

- A multi-population Cairns-Blake-Dowd model (M-CBD)

The M-CBD model is an extension of the original Cairns-Blake-Dowd model (Cairns

et al., 2006a). It can be expressed as

$$\ln \left(\frac{q_{x,t}^{(i)}}{1 - q_{x,t}^{(i)}} \right) = \kappa_{1,t}^* + \kappa_{2,t}^*(x - \bar{x}) + \kappa_{1,t}^{(i)} + \kappa_{2,t}^{(i)}(x - \bar{x}) + e_{x,t}^{(i)}, \quad i = 1, \dots, P,$$

where \bar{x} denotes the average age over the sample age range, $\kappa_{1,t}^*$ and $\kappa_{2,t}^*$ are time-varying parameters that are shared by all P populations, $\kappa_{1,t}^{(i)}$ and $\kappa_{2,t}^{(i)}$ are time-varying parameters that apply only to population i , and $e_{x,t}^{(i)}$ is the error term. We estimate the M-CBD model to data from EW males and UK male insured lives with the method of least squares.

The vector of $\kappa_{1,t}^*$ and $\kappa_{2,t}^*$ is modeled by a bivariate random walk with drift. Each $\kappa_{1,t}^{(i)}$ is modeled by a first order autoregression, with a mean-reverting property that ensures the resulting projection is coherent.

The hedge effectiveness under the alternative simulation models is calculated with the procedure below.

1. Generate N mortality scenarios from either the M-LC or M-CBD model.
2. For each mortality scenario and $t = 1, \dots, Y$,
 - (a) calculate the values of $S_{x_0,0}^{(H)}(s)$, $s = 1, \dots, t$, in PL_t by using equation (2.1) and the simulated death probabilities;
 - (b) estimate the realized values of K_t , $k_t^{(H)}$ and $k_t^{(R)}$ by minimizing the following

sum of squares:

$$\sum_x \left(\ln(\tilde{m}_{x,t}^{(i)}) - \hat{a}_x^{(i)} - \hat{B}_x K_t - \hat{b}_x^{(i)} k_t^{(i)} \right)^2, \quad i = H, R,$$

where $\tilde{m}_{x,t}^{(i)}$ denotes the value of $m_{x,t}^{(i)}$ simulated from the alternative model, and $\hat{a}_x^{(i)}$, \hat{B}_x and $\hat{b}_x^{(i)}$ are the estimates of $a_x^{(i)}$, B_x and $b_x^{(i)}$ in the assumed ACF model, respectively;

(c) using the values of K_t , $k_t^{(H)}$ and $k_t^{(R)}$ obtained in step (b), compute FL_t , $Q_t(t)$, $\frac{\partial FL_t}{\partial K_t}$, $\frac{\partial Q_t(t)}{\partial K_t}$ and h_t ; the values of $D_{x,t,j}^{(i)}(T)$, $i = H, R$, $j = 0, \dots, 5$, involved in these quantities remain unchanged, because the valuation model is still the ACF model.

(d) using the results from steps (a) and (c), calculate PA_t and PL_t .

3. Calculate $\text{Var}(PA_t - PL_t | \mathcal{F}_0)$, $\text{Var}(PL_t | \mathcal{F}_0)$ and finally HE_t for $t = 1, \dots, Y$.

The middle and right panels in Figure 2.6 show the hedging results when the simulation model used is M-LC and M-CBD, respectively. For ease of comparison, the left panel in the same figure shows the baseline hedging result that is based on mortality scenarios generated from the ACF model.

The hedging result when the simulation model is M-LC is quite close to the baseline result. This outcome may be attributed to the fact that the ACF and M-LC models are similar. Both models are generalizations of the single-population Lee-Carter model, and both models contain only one time-varying factor that is shared by all populations being modeled. Also, as the M-LC model contains one less stochastic process than the ACF

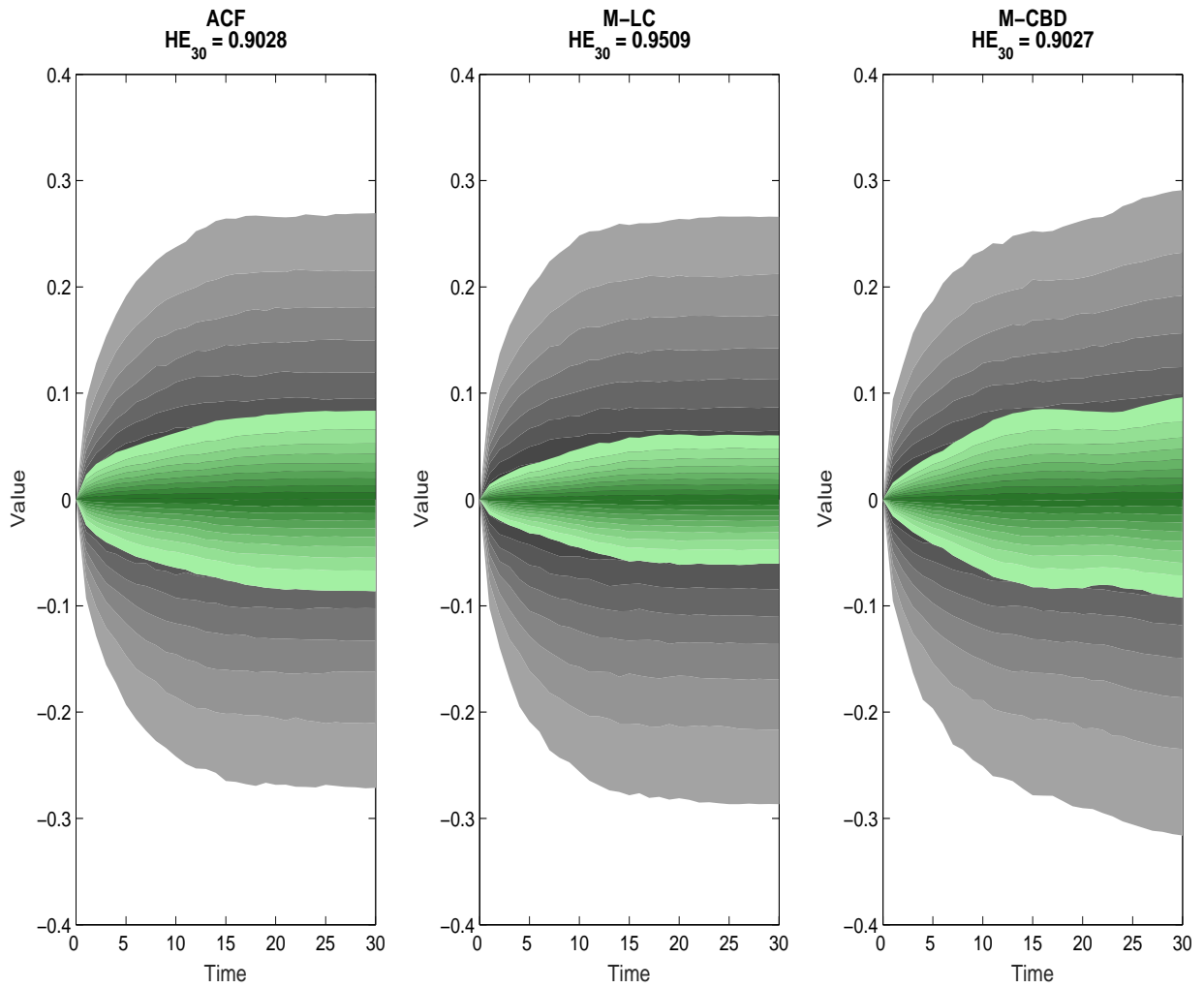


Figure 2.6: Fan charts showing the distributions of $(PL_t - PL_0)|\mathcal{F}_0$ (in gray) and $(PL_t - PA_t)|\mathcal{F}_0$ (in green) when the simulation models are ACF (the left panel), M-LC (the middle panel) and M-CBD (the right panel). The corresponding values of HE_{30} are displayed on the top of the diagrams.

model,¹¹ it may imply less stochastic uncertainty, which may explain why it leads to a hedging result that is even better than the baseline result.

The hedging result when the simulation model is M-CBD is not as good as the baseline result. This outcome may be explained by the fact that the M-CBD model contains two stochastic factors that are common to both populations, but the hedge is composed of only one instrument at a time. Nevertheless, the value of HE_{30} produced under this simulation model is still above 90%, indicating that the hedge remains highly effective even if the true underlying model is different and more sophisticated.

Robustness Relative to Small Sample Risk

Next, we investigate the impact of small sample risk (a.k.a. sampling risk and Poisson risk) on hedge effectiveness. The cohort of pensioners is now treated as a random survivorship group, so that given the values of l_{x_0+s-1} and $q_{x_0+s-1,s}^{(H)}$,

$$l_{x_0+s} \sim \text{Binomial}(l_{x_0+s-1}, 1 - q_{x_0+s-1,s}^{(H)}),$$

$s = 1, \dots, Y$, where l_x represents the number of pensioners who survive to age x . Note that l_{x_0} is non-random.

The procedure and assumptions for calculating hedge effectiveness remain the same, except that the values of $S_{x_0,0}^{(H)}(s)$, $s = 1, \dots, t$, in PL_t are now calculated with an additional

¹¹In this application, the ACF model contains three stochastic processes (one for K_t , one for $k_t^{(H)}$ and one for $k_t^{(R)}$), whereas the M-LC model contains two stochastic processes (one for $\kappa_t^{(R)}$ and another for $\kappa_t^{(H)} - \kappa_t^{(R)}$).

simulation routine. Specifically, for each of the N mortality scenarios generated, we simulate a realization of l_{x_0+s} using the above binomial process, and then calculate the realized value of $S_{x_0,0}^{(H)}(s)$ as $\tilde{l}_{x_0+s}/l_{x_0}$, where \tilde{l}_{x_0+s} denotes the realized value of l_{x_0+s} . Because small sample risk affects only the pension plan's realized mortality experience, the values of FL_t , $Q_t(t)$ and h_t are unaffected.

In Figure 2.7 we show the hedging results when the pension plan begins at time 0 with $l_{60} = 10,000, 3,000$ and $1,000$ individuals aged $x_0 = 60$. To ease comparison, also shown in the same figure is the baseline hedging result that is based on the assumption that there is no small sample risk.

The hedge effectiveness is still very high (HE_{30} is close to 90%) when $l_{60} = 10,000$. However, the impact of small sample risk becomes apparent as l_{60} reduces to 3,000. These observations are in line with the results produced by Li and Hardy (2011) who considered a static longevity hedge.

Although the impact of small sample risk is significant, we believe that it can be mitigated by an appropriately designed reinsurance treaty that is executed in tandem with the dynamic longevity hedge. The design of such a reinsurance treaty is detailed in Section 2.4.3.

Robustness Relative to the q-Forwards' Reference Age

In early stages of market development, the availability of q-forwards is likely to be limited. It is therefore important to understand how hedge effectiveness may change if the characteristics of the q-forwards used are different.

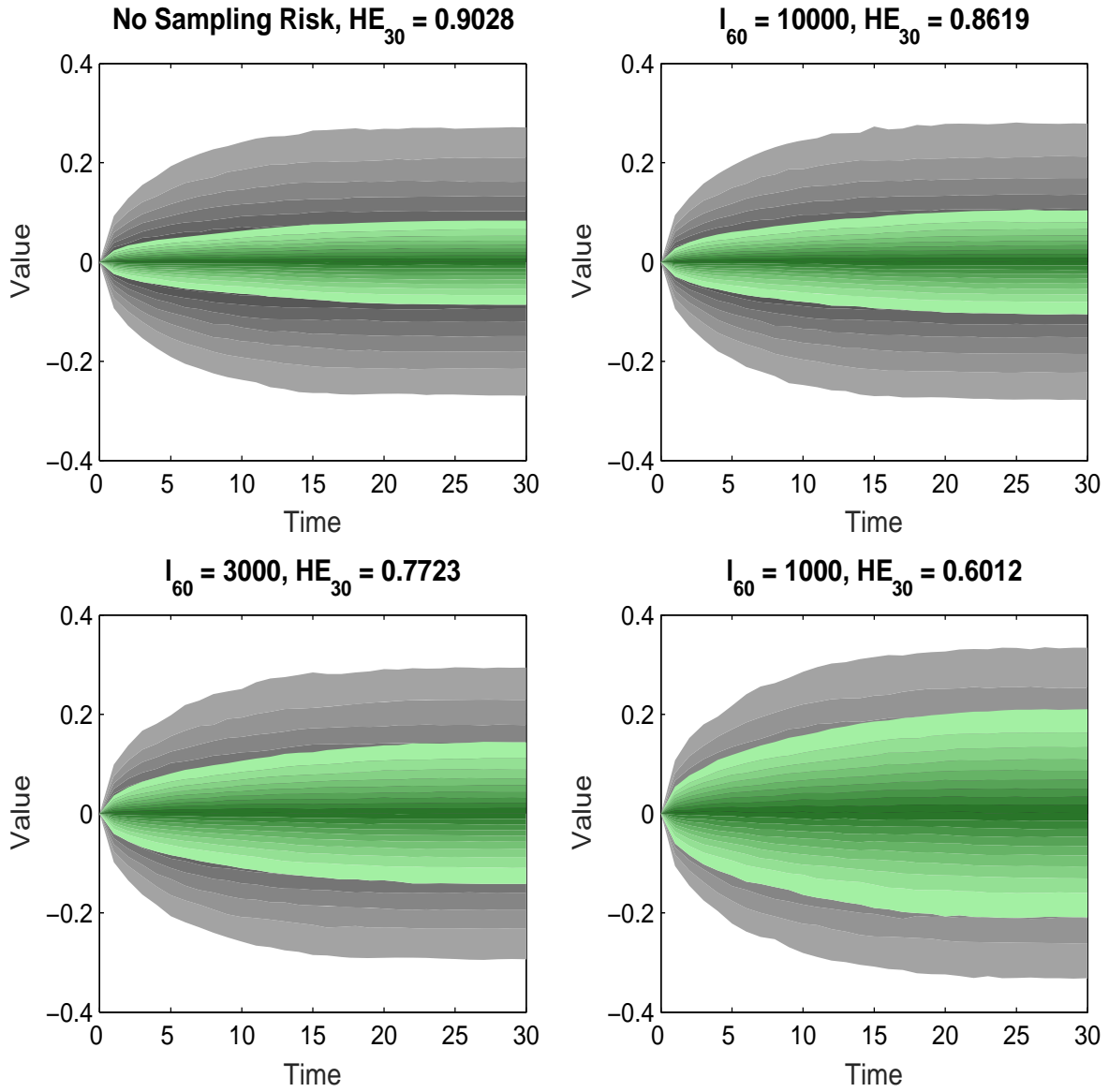


Figure 2.7: Fan charts showing the distributions of $(PL_t - PL_0)|\mathcal{F}_0$ (in gray) and $(PL_t - PA_t)|\mathcal{F}_0$ (in green) when $l_{60} = 10,000, 3,000, 1,000$ and when there is no small sample risk. The corresponding values of HE_{30} are displayed on the top of the diagrams.

We hereby test the robustness of the hedge effectiveness relative to the reference age x_f of the q-forwards used. Figure 2.8 shows the hedging results when $x_f = 65, 70, 75, 80$. It can be seen that changes in x_f have only a negligible effect on the hedging result. For all four choices of x_f , the values of HE_{30} are over 90%.

Recall that the dynamic longevity hedge is constructed by matching the sensitivities of the pension plan's liabilities and the hedge portfolio with respect to K_t . Therefore, a hedging instrument tends to be effective if its payoff is heavily dependent on the randomness associated with K_t (which affects both the hedging instrument and the liabilities being hedged) but not so much on the randomness associated with $k_t^{(H)}$ (which affects the hedging instrument but has little effect on the liabilities being hedged). In particular, for a q-forward with reference age x_f , the resulting hedge effectiveness tends to be high if

$$\text{Var}(B_{x_f} K_{t+T^*} | \mathcal{F}_t) \gg \text{Var}(b_{x_f}^{(H)} k_{t+T^*}^{(H)} | \mathcal{F}_t).$$

Given the parameter estimates, we have $B_{x_f} \gg b_{x_f}^{(H)}$ for $x_f = 65, \dots, 80$ and $\text{Var}(K_{t+T^*} | \mathcal{F}_t) = T^* \sigma_K^2 \gg \text{Var}(k_{t+T^*}^{(H)} | \mathcal{F}_t) = (1 - (\phi_1^{(H)})^{2T^*}) \sigma_{k,H}^2 / (1 - (\phi_1^{(H)})^2)$ for $T^* = 10$. Therefore, the relation above holds and the hedging results shown in Figure 2.8 are generally good. The four choices of x_f lead to slightly different hedging results, because there exist small variations in the estimates of B_x and $b_x^{(H)}$ over the age range of 65 to 80.

Robustness Relative to the q-Forwards' Time-to-Maturity

Finally, we study the robustness of the hedge effectiveness relative to the time-to-maturity T^* of the q-forwards used. We implement the dynamic longevity hedge using q-forwards

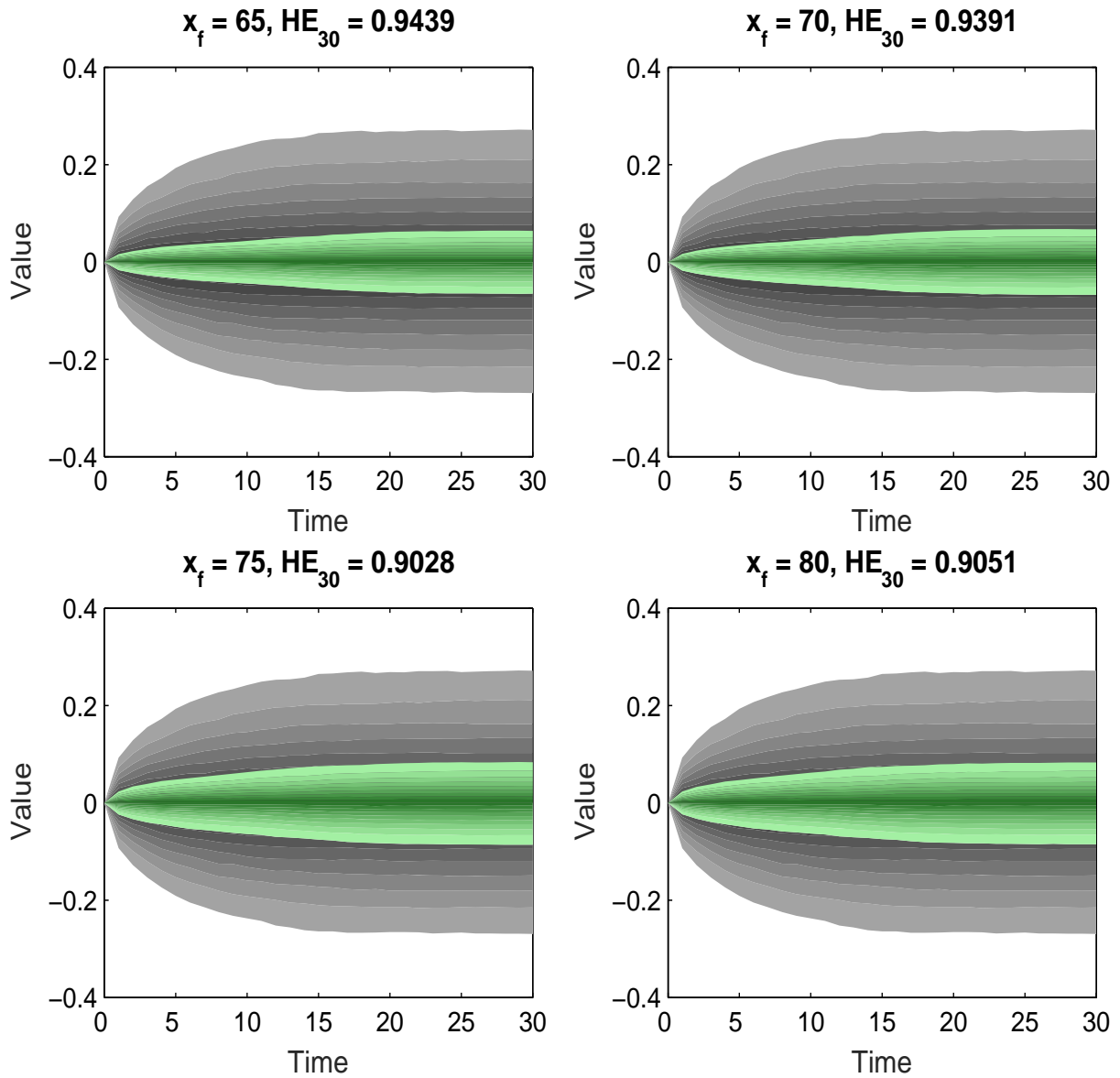


Figure 2.8: Fan charts showing the distributions of $(PL_t - PL_0)|\mathcal{F}_0$ (in gray) and $(PL_t - PA_t)|\mathcal{F}_0$ (in green) when $x_f = 65, 70, 75, 80$. The corresponding values of HE_{30} are displayed on the top of the diagrams.

with maturities of 5, 10, 15 and 20 years. The hedging results are displayed in Figure 2.9.

The dynamic longevity hedge is more effective when the q-forwards used have a longer time-to-maturity. This result is because as T^* increases, $\text{Var}(K_{t+T^*}|\mathcal{F}_t)$ grows linearly while $\text{Var}(k_{t+T^*}^{(H)}|\mathcal{F}_t)$ approaches gradually to a constant, which in turn means that the random underlying mortality rate becomes relatively more dependent on the randomness associated with K_t (which affects both the q-forward and the liabilities being hedged) but less on the randomness associated with $k_t^{(H)}$ (which has little effect on the liabilities being hedged).¹²

Still, even when T^* is as small as five years, the value of HE_{30} is higher than 80%. The high effectiveness can be attributed to the dynamic nature of our hedging strategy. Because we adjust the hedge annually and hold each q-forward for only one year, each q-forward is responsible for hedging the uncertainty that is one year ahead only. For this reason, short-dated q-forwards still lead to highly satisfactory results, despite the liability payments last for 30 years. This feature distinguishes our method from static hedging strategies, such as that in the next chapter or proposed in Li and Luo (2012), which generally require longer-dated instruments to achieve a satisfactory result.

2.4 Managing the Residual Risks

In this section, we explain how the residual risks from a dynamic, index-based longevity hedge can be managed through a reinsurance mechanism. We begin with a description of the assumptions used, followed by an exploratory analysis of the potential diversifiability of

¹²This property can be visualized from Figure A.1 in Appendix A.

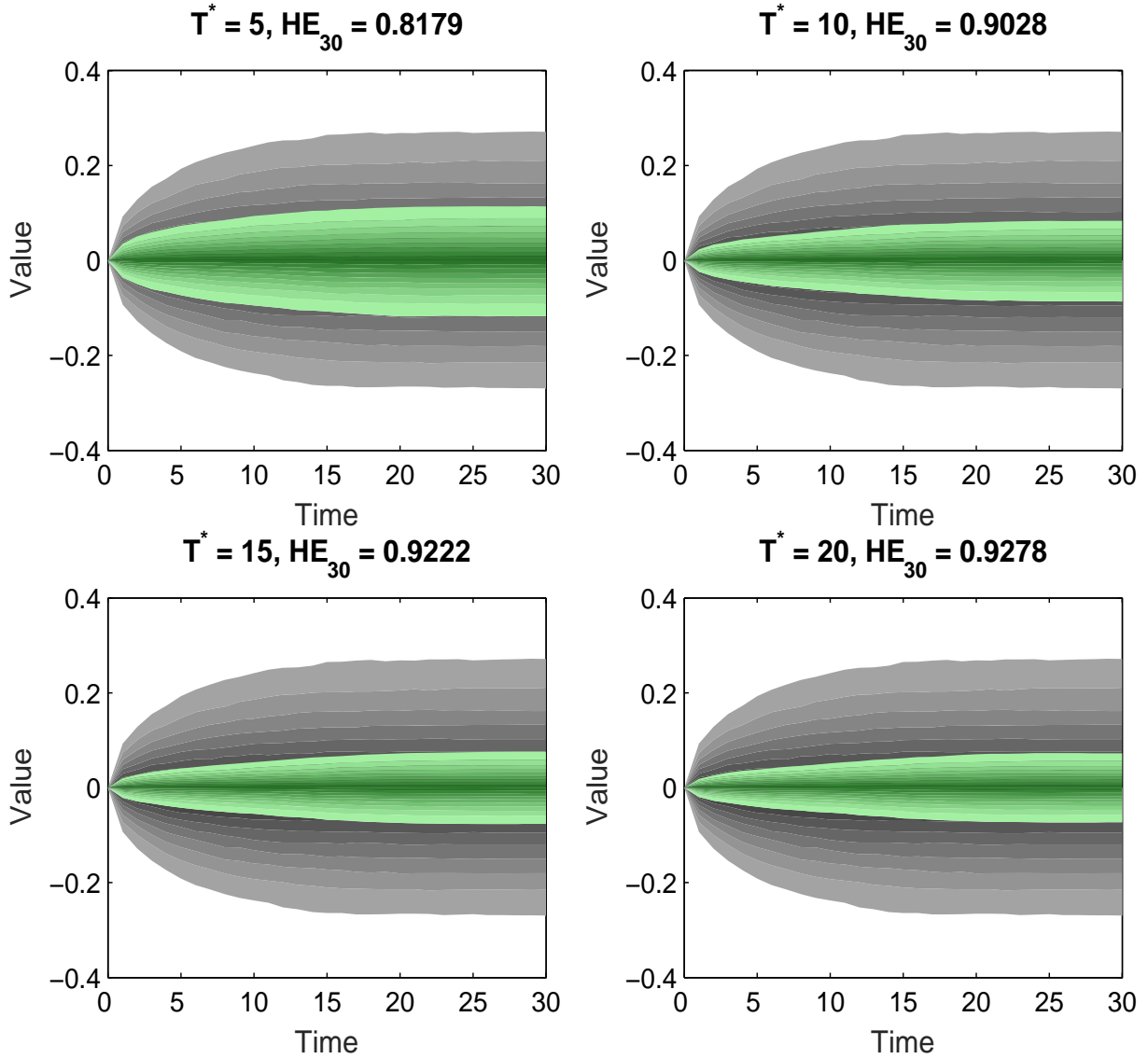


Figure 2.9: Fan charts showing the distributions of $(PL_t - PL_0)|\mathcal{F}_0$ (in gray) and $(PL_t - PA_t)|\mathcal{F}_0$ (in green) when $T^* = 5, 10, 15, 20$. The corresponding values of HE_{30} are displayed on the top of the diagrams.

the residual risks. We then define a reinsurance treaty which we call a ‘customized surplus swap’ and demonstrate how it works with real mortality data.

2.4.1 Assumptions

As we expand our analysis to include more than two populations, some of the previously made assumptions have to be modified accordingly. Below we list the assumptions that are used in this section.

- (i) There are 25 pension plans wishing to hedge their longevity risk exposures. The 25 pension plans have respectively identical mortality experience to the 25 male populations listed in Table 2.1. ¹³
- (ii) Each pension plan contains initially $l_{60} = 3,000$ pensioners who are all aged $x_0 = 60$. For $x = 61, 62, \dots, l_x$ follows the binomial process described in Section 2.3.3.
- (iii) At any time point during the hedging horizon, the only hedging instrument available is a q-forward that is linked to EW male population with a time-to-maturity (from inception) of $T^* = 10$ years and a reference age of $x_f = 75$.
- (iv) The values of $D_{x,t,j}^{(i)}(T)$ for $i = 1, \dots, 25$ and $j = 0, \dots, 5$ are computed from an ACF model that is estimated to the data from the 25 male populations listed in Table 2.1. ¹⁴

¹³The chosen 25 male populations are the same as the 25 populations that are classified as the ‘males West-cluster’ by Hatzopoulos and Haberman (2013).

¹⁴The mortality data for all 25 male populations are obtained from the Human Mortality Database (2014). The data used cover a sample period of 1959 to 2009 and a sample age range of 60 to 89.

Index (i)	Population	Index (i)	Population
1	England & Wales (EW)	14	Spain (ESP)
2	Scotland (SCO)	15	The United States (USA)
3	East Germany (DEUE)	16	Luxembourg (LUX)
4	West Germany (DEUW)	17	The Netherlands (NLD)
5	France (FRA)	18	Sweden (SWE)
6	Portugal (PRT)	19	Ireland (IRL)
7	Switzerland (CHE)	20	Norway (NOR)
8	Belgium (BEL)	21	Australia (AUS)
9	Finland (FIN)	22	Iceland (ISL)
10	Canada (CAN)	23	Japan (JPN)
11	Austria (AUT)	24	Czech (CZE)
12	Italy (ITA)	25	Denmark (DNK)
13	New Zealand (NZL)		

Table 2.1: The 25 male populations that are considered in Section 2.4.

- (v) To match the end point of the data sample period, time 0 is set to the end of year 2009.
- (vi) The evaluation of hedge effectiveness is based on $N = 10,000$ mortality scenarios that are generated from the model described in Assumption (iv).

Assumptions (2), (3), (5), (6) and (7) stated in Section 2.3.1 remain unchanged.

2.4.2 An Exploratory Analysis

Let us first study the hedging results for the 25 pension plans (see Figure 2.10). As expected, the hedging result for the plan associated with EW males is the best, because there is no population basis risk involved in the hedge. For the remaining 24 plans, the hedging results vary significantly, with HE_{30} ranging from 38% to 77%. The results indicate that the dynamic longevity hedge may leave substantial residual risks.

The residual risks include small sample risk and population basis risk. As small sample risk is inversely related to the number of individuals in a portfolio, it is quite obvious that it can be diversified away by pooling different pension plans. The diversifiability of population basis risk is not that apparent, but may be understood by comparing the correlation matrices which we now present.

In Table 2.2 we show the sample correlation coefficients of the log central death rates at age 75 for the 25 male populations listed in Table 2.1. In general, the correlation coefficients are very close to one, indicating the uncertainty surrounding the mortality rates of the 25

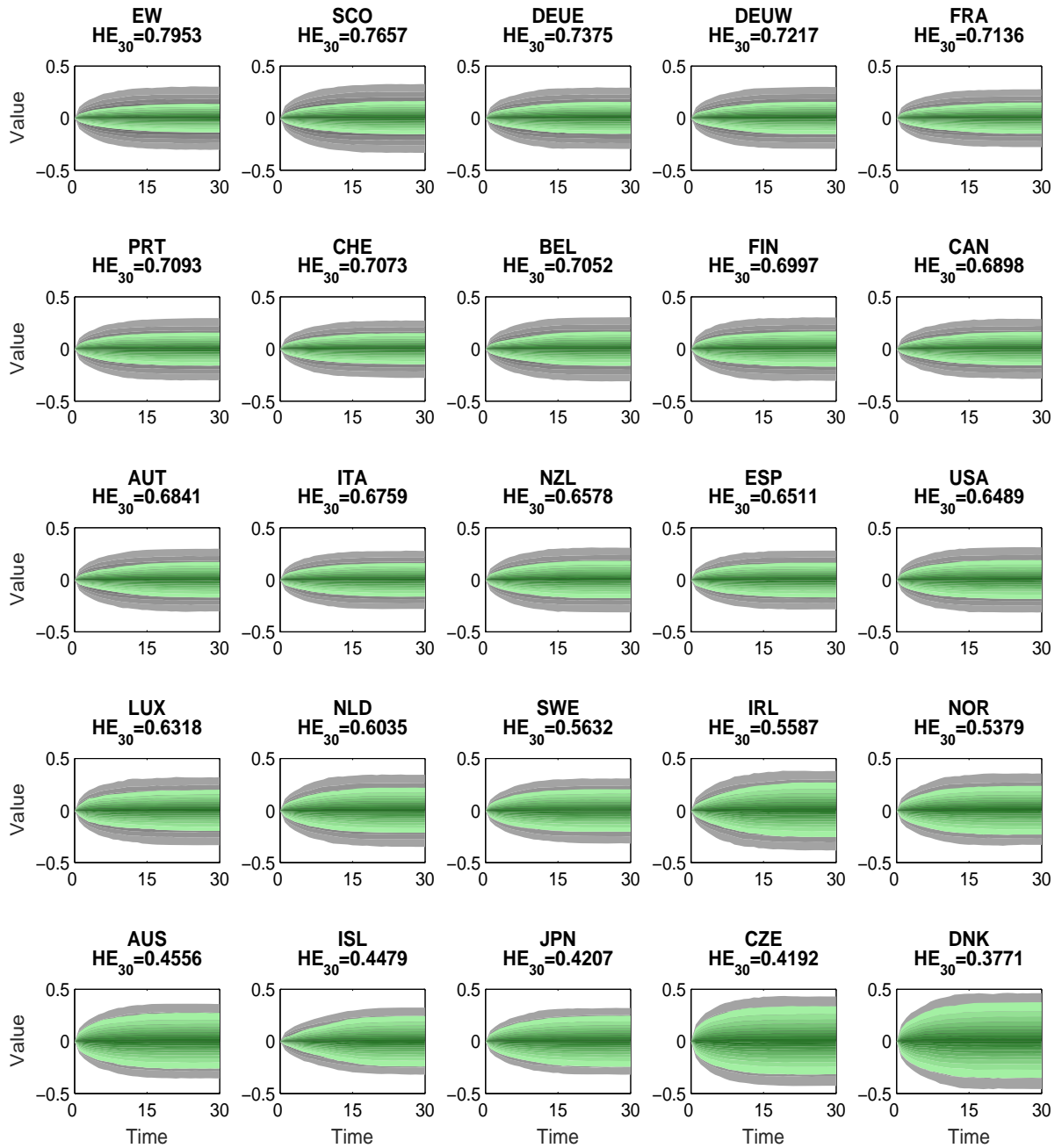


Figure 2.10: Fan charts showing the distributions of $(PL_t - PL_0)|\mathcal{F}_0$ (in gray) and $(PL_t - PA_t)|\mathcal{F}_0$ (in green) for the 25 pension plans under consideration. The corresponding values of HE_{30} are displayed on the top of the diagrams.

male populations is largely systematic. This result supports the use of an index-based hedge to remove the portion of longevity risk that is common to all populations.

In Table 2.3 we show the sample correlation coefficients of $\ln(m_{75,t}^{(i)}) - \hat{B}_{75}\hat{K}_t$, $i = 1, \dots, 25$, where \hat{B}_{75} and \hat{K}_t are respectively the estimates of B_{75} and K_t in the ACF model that is fitted to the data from the 25 male populations. We can interpret the quantity $\ln(m_{75,t}^{(i)}) - \hat{B}_{75}\hat{K}_t$ to mean the log central death rate at age 75 after removing the random component that is shared by all 25 male populations. Also, because the dynamic longevity hedge described in Section 2.2 is constructed to eliminate the uncertainty associated with the common trend K_t , we can understand the sample correlation coefficients in Table 2.3 as the residual correlations between the log mortality rates that are associated with the 25 pension plans after implementing the dynamic longevity hedge.

The off-diagonal portion of Table 2.3 contains a mixture of positive and negative values, with some quite close to zero. More importantly, they are significantly smaller than the corresponding values in Table 2.2. These observations suggest that the uncertainty not captured by the dynamic longevity hedge may possibly be diversified away by pooling different pension plans.

2.4.3 A Customized Surplus Swap

Motivated by the results of the exploratory analysis, we propose a customized surplus swap that permits pooling of the residual risks from different dynamic longevity hedges. When implementing such a swap in tandem with a dynamic index-based hedge, the pension plan would in theory be immunized from longevity risk.

	EW	SCO	DEUE	DEUW	FRA	PRT	CHE	BEL	FIN	CAN	AUT	ITA	NZL	ESP	USA	LUX	NLD	SWE	IRL	NOR	AUS	ISL	JPN	CZE	DNK
EW	1.00	0.98	0.98	0.99	0.91	0.97	0.99	0.98	0.96	0.99	0.93	0.98	0.95	0.98	0.99	0.95	0.98	0.92	0.92	0.89	0.98	0.97	0.89	0.68	0.98
SCO	0.98	1.00	0.97	0.97	0.90	0.97	0.98	0.96	0.95	0.98	0.94	0.97	0.94	0.96	0.97	0.94	0.97	0.90	0.91	0.88	0.97	0.96	0.89	0.66	0.97
DEUE	0.98	0.97	1.00	0.96	0.83	0.98	0.98	0.96	0.97	0.98	0.87	0.98	0.98	0.99	0.96	0.90	0.98	0.96	0.86	0.82	0.98	0.97	0.88	0.63	0.98
DEUW	0.99	0.97	0.96	1.00	0.92	0.95	0.98	0.97	0.95	0.98	0.93	0.97	0.93	0.96	0.98	0.94	0.99	0.89	0.93	0.89	0.98	0.96	0.90	0.67	0.99
FRA	0.91	0.90	0.83	0.92	1.00	0.85	0.89	0.89	0.84	0.91	0.96	0.86	0.78	0.84	0.92	0.94	0.89	0.70	0.95	0.94	0.88	0.88	0.83	0.69	0.89
PRT	0.97	0.97	0.98	0.95	0.85	1.00	0.98	0.96	0.96	0.97	0.89	0.98	0.96	0.98	0.96	0.91	0.96	0.95	0.85	0.85	0.97	0.97	0.88	0.66	0.96
CHE	0.99	0.98	0.98	0.98	0.89	0.98	1.00	0.98	0.96	0.98	0.92	0.98	0.96	0.98	0.98	0.93	0.98	0.93	0.89	0.88	0.98	0.98	0.89	0.68	0.98
BEL	0.98	0.96	0.96	0.97	0.89	0.96	0.98	1.00	0.95	0.97	0.93	0.97	0.94	0.97	0.97	0.93	0.96	0.91	0.90	0.87	0.96	0.96	0.88	0.73	0.96
FIN	0.96	0.95	0.97	0.95	0.84	0.96	0.96	0.95	1.00	0.96	0.88	0.97	0.97	0.98	0.95	0.88	0.97	0.94	0.86	0.82	0.97	0.95	0.84	0.64	0.97
CAN	0.99	0.98	0.98	0.98	0.91	0.97	0.98	0.97	0.96	1.00	0.93	0.97	0.95	0.97	0.98	0.94	0.99	0.91	0.93	0.88	0.99	0.96	0.89	0.66	0.99
AUT	0.93	0.94	0.87	0.93	0.96	0.89	0.92	0.93	0.88	0.93	1.00	0.89	0.84	0.88	0.94	0.95	0.92	0.76	0.95	0.92	0.92	0.91	0.84	0.72	0.92
ITA	0.98	0.97	0.98	0.97	0.86	0.98	0.98	0.97	0.97	0.97	0.89	1.00	0.97	0.99	0.97	0.91	0.97	0.95	0.87	0.84	0.98	0.97	0.88	0.66	0.97
NZL	0.95	0.94	0.98	0.93	0.78	0.96	0.96	0.94	0.97	0.95	0.84	0.97	1.00	0.98	0.93	0.85	0.95	0.97	0.80	0.76	0.96	0.95	0.85	0.60	0.95
ESP	0.98	0.96	0.99	0.96	0.84	0.98	0.98	0.97	0.98	0.97	0.88	0.99	0.98	1.00	0.96	0.90	0.97	0.96	0.85	0.83	0.97	0.97	0.86	0.65	0.97
USA	0.99	0.97	0.96	0.98	0.92	0.96	0.98	0.97	0.95	0.98	0.94	0.97	0.93	0.96	1.00	0.94	0.98	0.89	0.92	0.90	0.97	0.97	0.88	0.65	0.98
LUX	0.95	0.94	0.90	0.94	0.94	0.91	0.93	0.93	0.88	0.94	0.95	0.91	0.85	0.90	0.94	1.00	0.93	0.80	0.92	0.93	0.92	0.91	0.84	0.68	0.93
NLD	0.98	0.97	0.98	0.99	0.89	0.96	0.98	0.96	0.97	0.99	0.92	0.97	0.95	0.97	0.98	0.93	1.00	0.91	0.92	0.86	0.99	0.96	0.89	0.64	1.00
SWE	0.92	0.90	0.96	0.89	0.70	0.95	0.93	0.91	0.94	0.91	0.76	0.95	0.97	0.96	0.89	0.80	0.91	1.00	0.73	0.71	0.93	0.92	0.81	0.55	0.91
IRL	0.92	0.91	0.86	0.93	0.95	0.85	0.89	0.90	0.86	0.93	0.95	0.87	0.80	0.85	0.92	0.92	0.92	0.73	1.00	0.89	0.91	0.88	0.84	0.72	0.92
NOR	0.89	0.88	0.82	0.89	0.94	0.85	0.88	0.87	0.82	0.88	0.92	0.84	0.76	0.83	0.90	0.93	0.86	0.71	0.89	1.00	0.86	0.86	0.79	0.63	0.86
AUS	0.98	0.97	0.98	0.98	0.88	0.97	0.98	0.96	0.97	0.99	0.92	0.98	0.96	0.97	0.97	0.92	0.99	0.93	0.91	0.86	1.00	0.96	0.90	0.63	0.99
ISL	0.97	0.96	0.97	0.96	0.88	0.97	0.98	0.96	0.95	0.96	0.91	0.97	0.95	0.97	0.97	0.91	0.96	0.92	0.88	0.86	0.96	1.00	0.89	0.68	0.96
JPN	0.89	0.89	0.88	0.90	0.83	0.88	0.89	0.88	0.84	0.89	0.84	0.88	0.85	0.86	0.88	0.84	0.89	0.81	0.84	0.79	0.90	0.89	1.00	0.63	0.89
CZE	0.68	0.66	0.63	0.67	0.69	0.66	0.68	0.73	0.64	0.66	0.72	0.66	0.60	0.65	0.65	0.68	0.64	0.55	0.72	0.63	0.63	0.68	0.63	1.00	0.64
DNK	0.98	0.97	0.98	0.99	0.89	0.96	0.98	0.96	0.97	0.99	0.92	0.97	0.95	0.97	0.98	0.93	1.00	0.91	0.92	0.86	0.99	0.96	0.89	0.64	1.00

Table 2.2: The sample correlation coefficients of the log central death rates at age 75 for the 25 male populations under consideration.

	EW	SCO	DEUE	DEUW	FRA	PRT	CHE	BEL	FIN	CAN	AUT	ITA	NZL	ESP	USA	LUX	NLD	SWE	IRL	NOR	AUS	ISL	JPN	CZE	DNK
EW	1.00	0.36	0.13	0.59	0.30	0.00	0.27	0.44	0.01	0.55	0.34	0.14	-0.43	-0.23	0.54	0.61	0.56	-0.44	0.46	0.14	0.42	0.37	0.35	0.15	0.56
SCO	0.36	1.00	-0.35	0.58	0.79	-0.20	0.70	-0.20	0.16	0.63	0.81	-0.62	-0.00	0.45	0.66	0.65	0.29	-0.82	0.75	0.76	-0.11	0.08	0.17	0.38	0.29
DEUE	0.13	-0.35	1.00	-0.10	-0.54	0.08	-0.51	0.22	-0.00	0.16	-0.54	0.42	0.10	-0.37	-0.29	-0.27	0.38	0.50	-0.31	-0.57	0.44	0.10	0.22	-0.36	0.38
DEUW	0.59	0.58	-0.10	1.00	0.65	-0.35	0.56	0.11	0.04	0.72	0.64	-0.25	-0.19	0.22	0.70	0.61	0.69	-0.70	0.77	0.51	0.26	0.23	0.40	0.31	0.69
FRA	0.30	0.79	-0.54	0.65	1.00	-0.29	0.86	-0.24	0.20	0.60	0.93	-0.71	0.05	0.65	0.76	0.72	0.27	-0.92	0.88	0.94	-0.19	0.05	0.11	0.53	0.27
PRT	0.00	-0.20	0.08	-0.35	-0.29	1.00	-0.33	0.16	-0.35	-0.16	-0.28	0.32	-0.29	-0.45	-0.29	-0.05	-0.29	0.22	-0.29	-0.30	0.08	0.15	0.19	-0.12	-0.29
CHE	0.27	0.70	-0.51	0.56	0.86	-0.33	1.00	-0.19	0.08	0.50	0.82	-0.70	0.09	0.62	0.72	0.61	0.16	-0.76	0.73	0.86	-0.19	0.10	0.11	0.52	0.16
BEL	0.44	-0.20	0.22	0.11	-0.24	0.16	-0.19	1.00	-0.19	0.07	-0.09	0.60	-0.47	-0.51	0.05	0.11	0.21	0.04	-0.02	-0.38	0.38	0.31	0.26	0.14	0.21
FIN	0.01	0.16	-0.00	0.04	0.20	-0.35	0.08	-0.19	1.00	0.20	0.24	-0.18	0.34	0.32	0.13	0.04	0.27	-0.18	0.23	0.19	0.08	-0.06	-0.21	0.12	0.27
CAN	0.55	0.63	0.16	0.72	0.60	-0.16	0.50	0.07	0.20	1.00	0.58	-0.30	-0.10	0.23	0.61	0.64	0.74	-0.62	0.75	0.47	0.37	0.16	0.31	0.23	0.74
AUT	0.34	0.81	-0.54	0.64	0.93	-0.28	0.82	-0.09	0.24	0.58	1.00	-0.62	-0.02	0.53	0.78	0.75	0.29	-0.91	0.88	0.86	-0.07	0.15	0.10	0.56	0.29
ITA	0.14	-0.62	0.42	-0.25	-0.71	0.32	-0.70	0.60	-0.18	-0.30	-0.62	1.00	-0.36	-0.71	-0.39	-0.31	0.07	0.51	-0.49	-0.80	0.49	0.18	0.14	-0.35	0.07
NZL	-0.43	-0.00	0.10	-0.19	0.05	-0.29	0.09	-0.47	0.34	-0.10	-0.02	-0.36	1.00	0.41	-0.06	-0.23	-0.15	0.14	-0.07	0.10	-0.29	-0.13	-0.09	-0.07	-0.15
ESP	-0.23	0.45	-0.37	0.22	0.65	-0.45	0.62	-0.51	0.32	0.23	0.53	-0.71	0.41	1.00	0.42	0.26	-0.03	-0.48	0.43	0.71	-0.47	-0.24	-0.20	0.34	-0.03
USA	0.54	0.66	-0.29	0.70	0.76	-0.29	0.72	0.05	0.13	0.61	0.78	-0.39	-0.06	0.42	1.00	0.67	0.45	-0.75	0.75	0.67	0.10	0.25	0.20	0.30	0.45
LUX	0.61	0.65	-0.27	0.61	0.72	-0.05	0.61	0.11	0.04	0.64	0.75	-0.31	-0.23	0.26	0.67	1.00	0.37	-0.78	0.73	0.65	0.08	0.17	0.17	0.40	0.37
NLD	0.56	0.29	0.38	0.69	0.27	-0.29	0.16	0.21	0.27	0.74	0.29	0.07	-0.15	-0.03	0.45	0.37	1.00	-0.36	0.52	0.11	0.62	0.11	0.35	-0.03	1.00
SWE	-0.44	-0.82	0.50	-0.70	-0.92	0.22	-0.76	0.04	-0.18	-0.62	-0.91	0.51	0.14	-0.48	-0.75	-0.78	-0.36	1.00	-0.87	-0.81	0.09	-0.11	-0.17	-0.55	-0.36
IRL	0.46	0.75	-0.31	0.77	0.88	-0.29	0.73	-0.02	0.23	0.75	0.88	-0.49	-0.07	0.43	0.75	0.73	0.52	-0.87	1.00	0.77	0.10	0.14	0.22	0.56	0.52
NOR	0.14	0.76	-0.57	0.51	0.94	-0.30	0.86	-0.38	0.19	0.47	0.86	-0.80	0.10	0.71	0.67	0.65	0.11	-0.81	0.77	1.00	-0.31	-0.02	-0.00	0.47	0.11
AUS	0.42	-0.11	0.44	0.26	-0.19	0.08	-0.19	0.38	0.08	0.37	-0.07	0.49	-0.29	-0.47	0.10	0.08	0.62	0.09	0.10	-0.31	1.00	0.23	0.37	-0.28	0.62
ISL	0.37	0.08	0.10	0.23	0.05	0.15	0.10	0.31	-0.06	0.16	0.15	0.18	-0.13	-0.24	0.25	0.17	0.11	-0.11	0.14	-0.02	0.23	1.00	0.37	0.14	0.11
JPN	0.35	0.17	0.22	0.40	0.11	0.19	0.11	0.26	-0.21	0.31	0.10	0.14	-0.09	-0.20	0.20	0.17	0.35	-0.17	0.22	-0.00	0.37	0.37	1.00	0.09	0.35
CZE	0.15	0.38	-0.36	0.31	0.53	-0.12	0.52	0.14	0.12	0.23	0.56	-0.35	-0.07	0.34	0.30	0.40	-0.03	-0.55	0.56	0.47	-0.28	0.14	0.09	1.00	-0.03
DNK	0.56	0.29	0.38	0.69	0.27	-0.29	0.16	0.21	0.27	0.74	0.29	0.07	-0.15	-0.03	0.45	0.37	1.00	-0.36	0.52	0.11	0.62	0.11	0.35	-0.03	1.00

Table 2.3: The sample correlation coefficients of the log central death rates at age 75 less the common time trend (i.e., $\ln(m_{75,t}^{(i)}) - \hat{B}_{75}\hat{K}_t$) for the 25 male populations under consideration.

A pension plan is immunized from longevity risk over the hedging horizon if $PA_t - PL_t = 0$ for $t = 1, \dots, Y$. We can regard $|PA_t - PL_t|$ as the pension plan's surplus if $PA_t > PL_t$ and short fall in assets if $PA_t < PL_t$. The swap we design has a maturity of one year and is written at each time point when the dynamic index-based hedge is established or adjusted. We call it a 'surplus' swap, because its net cash flow at maturity is derived from the surplus process $PA_t - PL_t$, $t = 1, \dots, Y$, of the pension plan.

Our goal is to ensure that $PA_t - PL_t = 0$ for $t = 1, \dots, Y$. We let NCF_t be the net cash flow (payable at time t from the reinsurer to the pension plan) for the customized surplus swap that is written at time $t - 1$. With the swap in place, the recursion formula for PA_t can be rewritten as

$$PA_t = PA_{t-1} + (1+r)^{-t}(h_{t-1}Q_t(t-1) + NCF_t), \quad t = 1, \dots, Y, \quad (2.3)$$

where $PA_0 = PL_0$. Using equations (2.3) and (2.2), we obtain

$$\begin{aligned} PL_t - PA_t &= PL_{t-1} - PA_{t-1} + (1+r)^{-t}(S_{x_0,0}^{(H)}(t)(1 + FL_t) - (1+r)S_{x_0,0}^{(H)}(t-1)FL_{t-1}) \\ &\quad - (1+r)^{-t}(h_{t-1}Q_t(t-1) + NCF_t), \quad t = 1, \dots, Y. \end{aligned}$$

To stipulate $PA_t - PL_t = 0$ for $t = 1, \dots, Y$, we require

$$NCF_t = S_{x_0,0}^{(H)}(t)(1 + FL_t) - h_{t-1}Q_t(t-1) - (1+r)S_{x_0,0}^{(H)}(t-1)FL_{t-1}, \quad t = 1, \dots, Y.$$

The expression for NCF_t is intuitive. It says that there is no net cash flow from the swap

if what the pension plan has at time $t - 1$ accumulated with interest (i.e., $(1 + r)S_{x_0,0}^{(H)}(t - 1)FL_{t-1}$) plus the proceed from the index-based hedge at time t (i.e., $h_{t-1}Q_t(t - 1)$) is just sufficient to cover the plan's financial obligations at time t (i.e., $S_{x_0,0}^{(H)}(t)$) and beyond (i.e., $S_{x_0,0}^{(H)}(t)FL_t$).

Given \mathcal{F}_{t-1} , the value of $(1 + r)S_{x_0,0}^{(H)}(t - 1)FL_{t-1}$ is known, but the values of $S_{x_0,0}^{(H)}(t)(1 + FL_t)$ and $h_{t-1}Q_t(t - 1)$ are random as they both depend on the values of K_t , $k_t^{(H)}$ and $k_t^{(R)}$ which are not known until time t . It follows that for a customized surplus swap written at time $t - 1$, the fixed and floating legs should be set to $(1 + r)S_{x_0,0}^{(H)}(t - 1)FL_{t-1}$ and $S_{x_0,0}^{(H)}(t)(1 + FL_t) - h_{t-1}Q_t(t - 1)$, respectively. The exchange of cash flows at maturity (time t) is illustrated diagrammatically in Figure 2.11.

Given how the cash flows are defined, the following should be incorporated into the terms of a customized surplus swap written at time $t - 1$:

- the method and assumptions used to calculate FL_{t-1} and FL_t ;
- the hedge ratio h_{t-1} ;
- the rate r at which the cash flows are discounted;
- the forward mortality rate q^f associated with the q-forward written at time $t - 1$.

For simplicity, we assume that the swap is costless in the following illustration. In practice, of course, the reinsurer demands a reward for taking on the risk and therefore a fixed payment (the risk premium) has to be paid by the pension plan to the reinsurer at either inception or maturity.

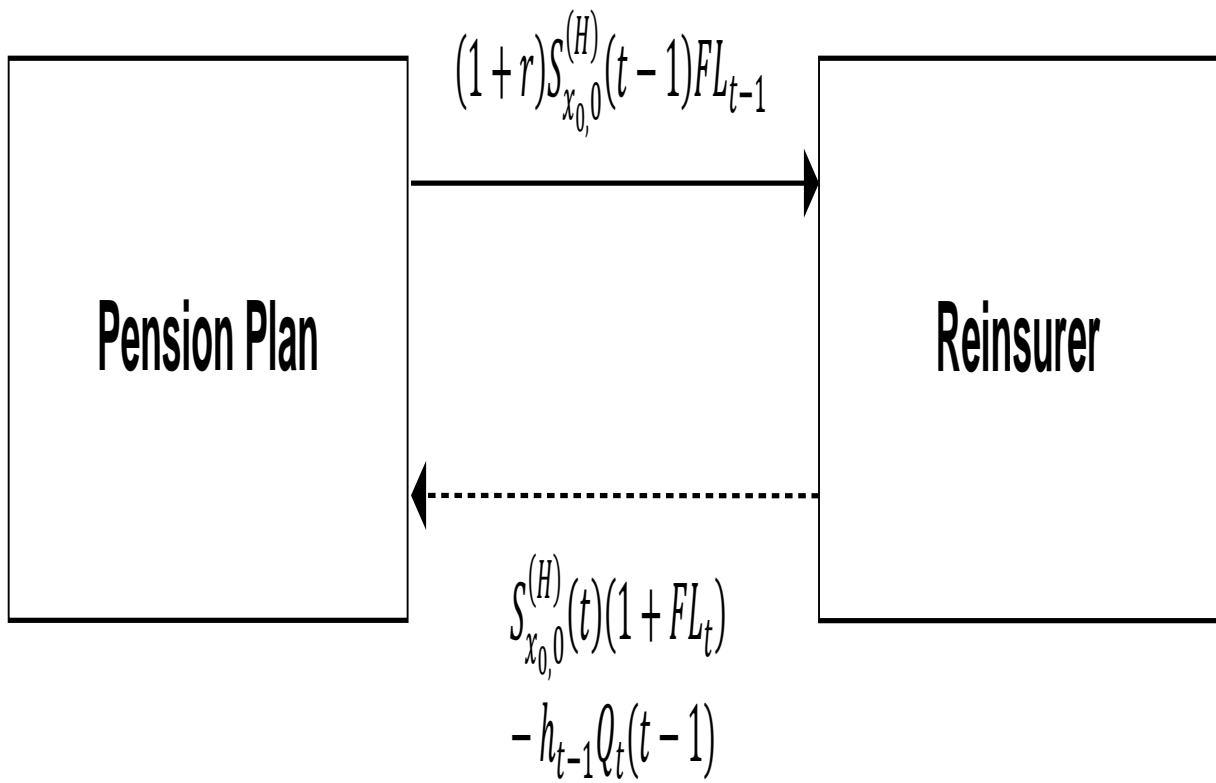


Figure 2.11: An illustration of the exchange of cash flows between the pension plan and reinsurer at time t when the customized surplus swap written at time $t - 1$ matures.

2.4.4 An Illustration

We now revisit the index-based longevity hedges for the 25 pension plans. Let us suppose that on top of the index-based hedges, all 25 pension plans write customized surplus swaps with the same reinsurer to eliminate their exposures to the residual risks. Assume further that the assumptions used in formulating the index-based hedges also apply to the terms of the customized surplus swaps.

The fan charts in Figure 2.12 show the distributions of $NCF_t|\mathcal{F}_0$ for the 25 pension plans. They are in line with the hedging results presented in Figure 2.10: the more effective the index-based hedge is, the less variable NCF_t is.

To study the diversifiability of the residual risks from the index-based hedges, let us consider the cash flows from the viewpoint of the reinsurer who writes customized surplus swaps with the 25 pension plans. The fan chart in Figure 2.13 depicts the distributions (conditioned on \mathcal{F}_0) of the average net cash flows payable to each pension plan over the hedging horizon. The variability of the reinsurer's average net cash flows is small compared to the variability of NCF_t for individual pension plans. The diversifiability can be observed more clearly from Figure 2.14, which compares the variances of the reinsurer's average net cash flows with the variances of the net cash flows arising from individual customized surplus swaps.

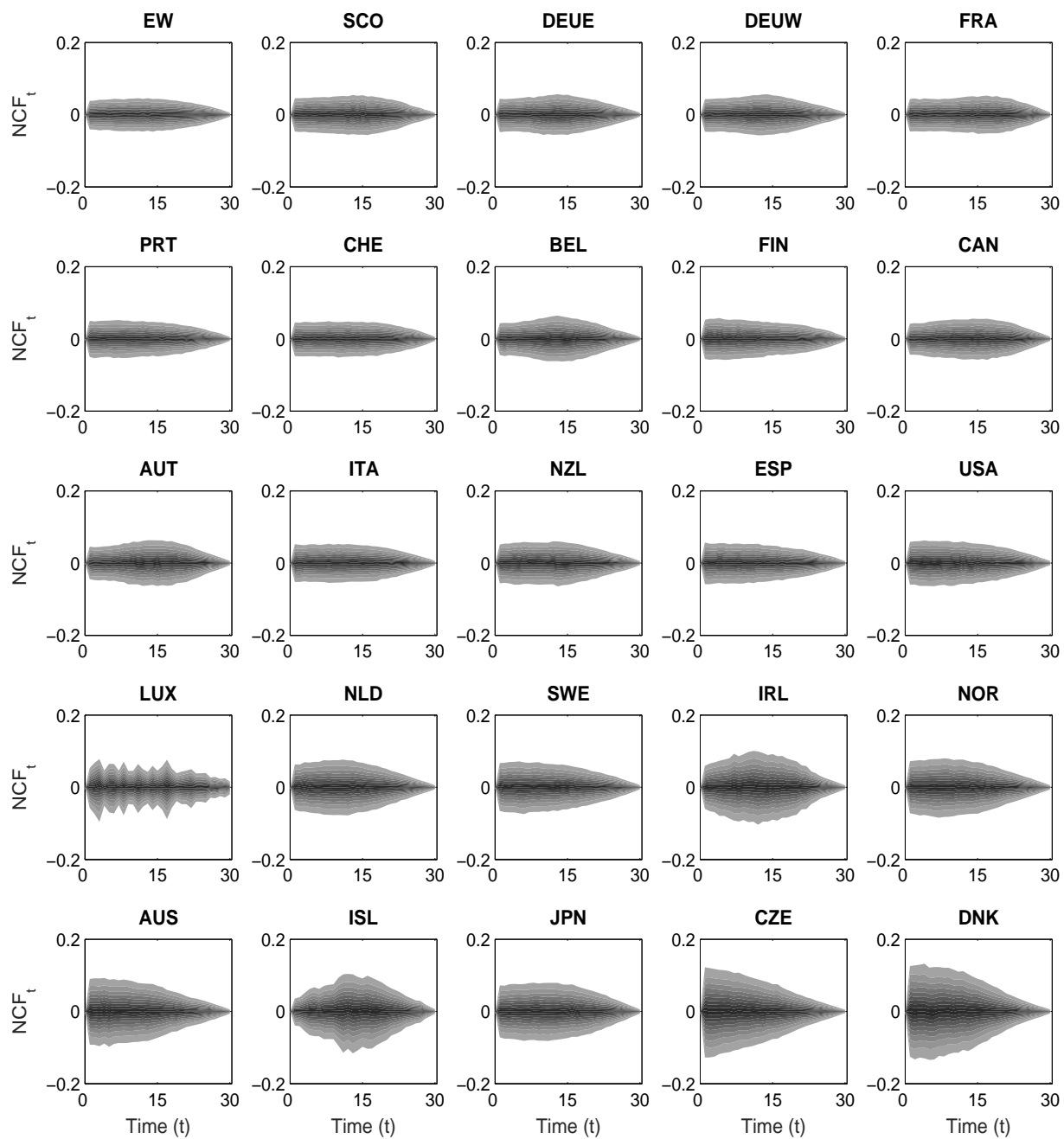


Figure 2.12: Fan charts showing the distributions of $NCF_t|\mathcal{F}_0$ for the 25 pension plans under consideration.

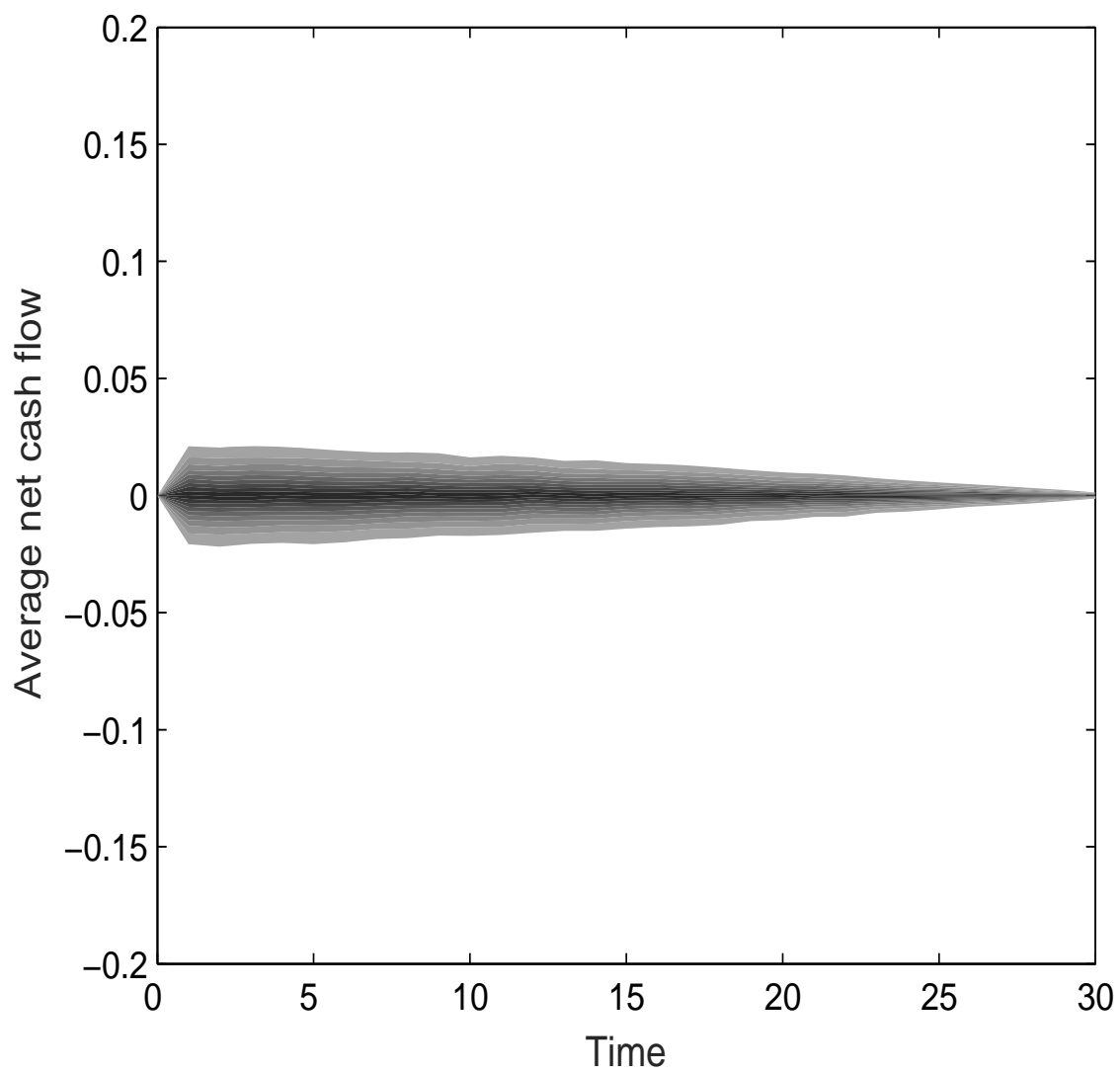


Figure 2.13: The distributions (conditioned on \mathcal{F}_0) of the average net cash flows payable from the reinsurer to each pension plan over the hedging horizon.

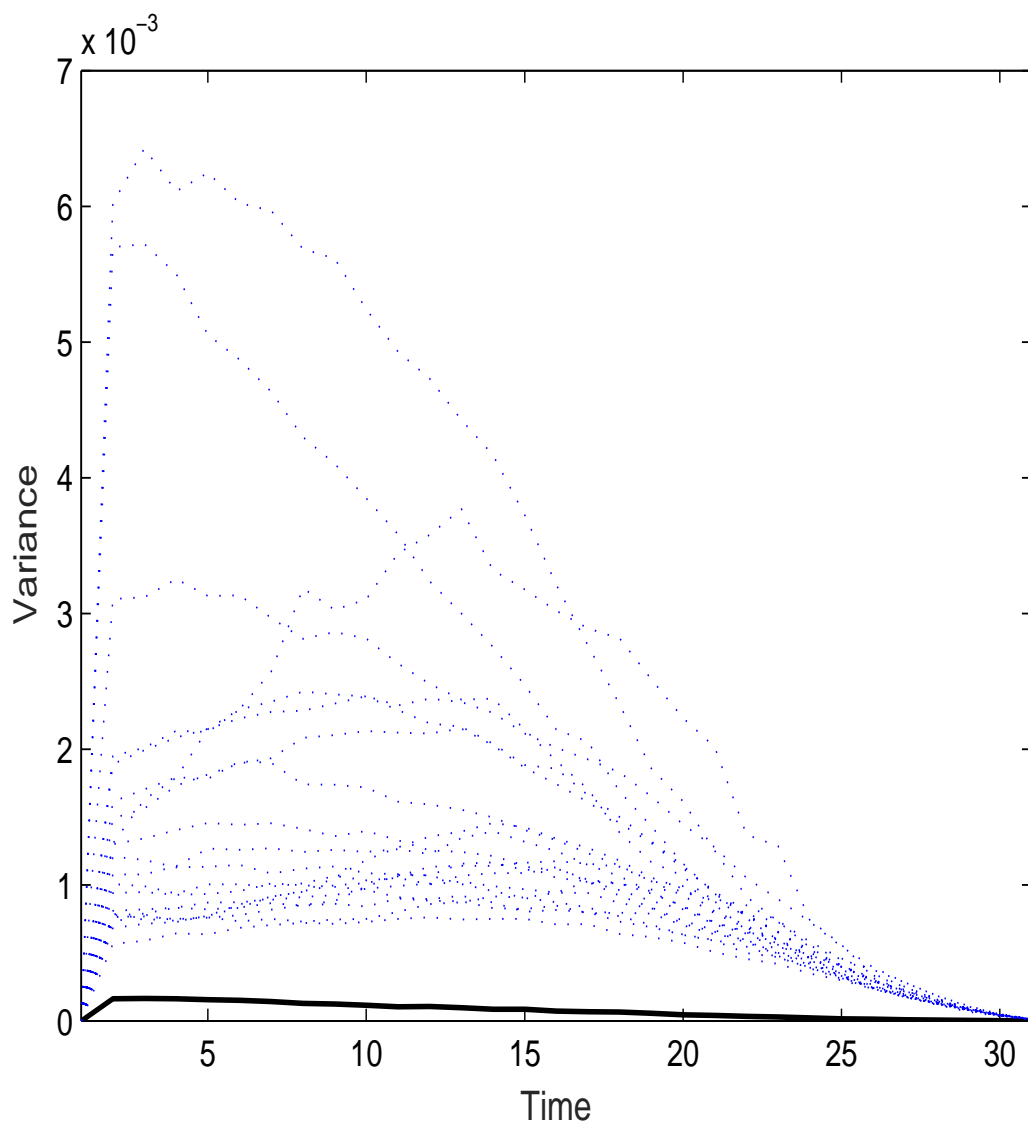


Figure 2.14: The values of $\text{Var}(NCF_t|\mathcal{F}_0)$, $t = 1, \dots, 30$, for the individual customized surplus swaps (the dotted lines) and the corresponding variances of the reinsurer's average net cash flows payable to each pension plan (the solid line).

2.5 Discussion and Conclusion

In this chapter, we consider a risk management framework in which longevity risk is split into trend risk and residual risks. With the proposed dynamic hedging strategy, a pension plan can transfer its trend risk exposure to capital markets through standardized instruments. Using the proposed customized surplus swap, the pension plan may also transfer the residual risks left behind by the dynamic hedge to a reinsurer, who collectively manages the residual risks from various pension plans. As a whole, our risk management framework allows pension plans to completely eliminate their longevity risk exposures, just as what they can achieve from traditional, entirely insurance-based pension de-risking solutions.

What we propose allows the longevity risk transfer market to package the trend risk as standardized securities that are structured like typical capital market derivatives. Compared to products such as pension buy-ins, standardized longevity-linked derivatives are more appealing to capital market investors who generally desire liquidity and transparency. When put in practice, our risk management framework may attract participation from capital markets, thereby ameliorating the demand and supply imbalance in the present market for longevity risk transfers. The enhancement of liquidity through standardization may also result in lower risk management costs to pension plans, as the illiquidity premium payable to the counterparty can be reduced. Although there is no sufficient data to test the inverse relationship between liquidity and compensation to investors (typically measured by the Sharpe ratio) in the longevity risk market, there is profound evidence for such an inverse relationship in several financial markets.

For stock markets, the inverse relationship between liquidity and risk-adjusted rate

of return was identified by Lo et al. (2003), who introduced liquidity to the standard mean-variance portfolio optimization framework by constructing three-dimensional mean-variance-liquidity frontiers on the basis of several measures of liquidity including trading volume and percentage bid/offer spreads. They studied the tangency portfolios of the liquidity-constrained mean-variance-liquidity efficient frontiers for some randomly selected stocks, and found that the Sharpe ratio of the tangency portfolio reduces as the liquidity threshold becomes less stringent.

For mutual fund markets, the relationship between liquidity and risk-adjusted rate of return was revealed by Idzorek et al. (2012), who investigated whether mutual funds that hold less liquid stocks tend to outperform those that hold more liquid stocks. They first grouped the population of mutual funds under consideration by size and valuation, and further categorized the funds in each group into five liquidity levels on the basis of the stock-level ‘turnover’ measure. It was found that, on average, mutual funds that held less liquid stocks possessed higher Sharpe ratios than those that held more liquid stocks.

For hedge fund markets, Getmansky et al. (2004) studied the potential relationship between liquidity and returns on hedge funds by developing an econometric model from which smoothing-adjusted Sharpe ratios were calculated. It was found that among 908 hedge funds from the TASS Hedge Fund Combined databases, the most illiquid hedge funds (e.g., fixed income directional) had the highest smoothing-adjusted Sharpe ratios, supporting the inverse relationship between liquidity and risk-adjusted required rate of return.

It has been argued that the market for longevity risk transfers has many similarities

compared to a typical financial market (Loeys et al., 2007). Hence, it is reasonable to conjecture that the inverse relationship between liquidity and Sharpe ratio found in stock, mutual fund and hedge fund markets also applies to the market for longevity risk transfers. Should this conjecture holds, then our risk management framework would be more economical than the comparable entirely insurance-based methods, because it could transfer the trend risk at a lower cost. A reduced cost may encourage more pension plans to transfer their longevity risk exposures, thereby not only facilitating market growth but also strengthening the stability of the pension industry.

To focus on the design and execution of the proposed risk management methods, we have made no attempt to estimate the associated costs. It thus warrants further studies to investigate how much the proposed risk management methods may cost. To determine the cost associated with the dynamic longevity hedge, one may replace q^f with a forward mortality rate that is derived from the pricing methods proposed by Chuang and Brockett (2014), Deng et al. (2012) and Li et al. (2011). As a reinsurance treaty, the customized surplus swap may be priced under the Solvency II framework. In particular, its profit margin may be calculated by multiplying the present value of the solvency capital requirements with the spread over risk-free rate which the reinsurer is required to earn on its equity (see Zhou et al., 2014). Also, to understand the value for money of our risk management framework, it would be interesting to compare the total cost required by the proposed risk management methods with that required by a full pension buy-out.¹⁵

As the proposed dynamic hedging strategy matches only the first partial derivatives

¹⁵Mercer provides pension buy-out indexes, which track the estimated cost of a full pension buy-out in the US, the UK, Ireland and Canada over time.

(with respect to the common time trend K_t), it requires the hedger to hold only one hedging instrument at a time. This property may be seen as advantageous, because it helps the market to concentrate liquidity. In future research, it may be fruitful to extend the proposed dynamic hedging strategy to match also the higher order derivatives, and to investigate whether such an extension would lead to an improvement in hedge effectiveness that worths the dilution of liquidity arising from the use of additional instruments.

The results of various robustness tests indicate that the effectiveness of the dynamic longevity hedge is reasonably robust relative to model risk, small sample risk, the q-forwards' reference age and the q-forwards' time-to-maturity. They also offer some useful insights to market participants. For example, because the dynamic hedge still yields satisfactory hedging results even if the time-to-maturity of the q-forwards is only five years, the market may choose to launch shorter-dated q-forwards, which are more likely to attract capital market investors. As robustness is important in gaining trust from various stakeholders, we believe that future research warrants a more extensive analysis of robustness which considers additional aspects of the longevity hedge (e.g., hedge ratios) and additional factors that may affect hedge effectiveness (e.g., parameter risk).

In illustrating the customized surplus swap, mortality data from a group of distinct national populations are used. In reality, however, a reinsurer may possibly write customized surplus swaps with pension plans that are located in the same country, so it is also important to understand the diversifiability of residual risks across sub-populations with the similar geographical locations but different social-economic statuses. Such an understanding may be developed by considering the Club Vita data set of UK occupational pension schemes that was used by Haberman et al. (2014).

Appendices

Appendix A

Evaluating the Quality of the Approximation Methods

In this appendix, we evaluate the quality of the methods used to approximate $p_{x,u}^{(i)}(T, K_t, k_t^{(i)})$.

The evaluation is based on the ACF model that is fitted to data from EW males and UK male insured lives. As in Section 2.3, in the following discussion we assume that the hedger's population (H) is UK male insured lives whereas the q-forwards' reference population (R) is EW males.

Let us first consider the quadratic approximation method for the situation when $u = t$ (Section 2.2.3). This approximation method is used when calculating FL_t and its derivatives, which are functions of $p_{x_0,t}^{(H)}(s, K_t, k_t^{(H)})$ for $s = 1, 2, \dots$. For brevity, we present the evaluation results for $p_{x_0,t}^{(H)}(s, K_t, k_t^{(H)})$ computed at $t = 5$, $x_0 = 60$ and $s = 5, 10, 20$ only. The evaluation results for other combinations of t , x_0 and s are similar.

The evaluation results for the chosen values of t , x_0 and s are shown graphically in Figure A.1. The dots in the diagrams represent 1,000 simulated pairs of $(K_5, k_5^{(H)})$ given \mathcal{F}_0 . The cloud of dots may therefore be seen as the possible range of $(K_5, k_5^{(H)})$. The centroid of the cloud represents $(\hat{K}_5, \hat{k}_5^{(H)})$, where, by definition, the approximation is exact.

In the left panels, the solid contour lines represent the ‘actual’ values that are calculated by full simulations on the basis of values of K_5 ranging from -30 to -5 and $k_5^{(H)}$ ranging from -0.3 to 0.3 . The dashed contour lines represent the approximated values that are computed by using the quadratic approximation formula derived in Section 2.2.3. The gap between each pair of dashed and solid contour lines is very narrow, indicating that the quadratic approximation is highly accurate.

The degree of accuracy may also be assessed from the right panels, in which the contour lines represent the percentage errors in approximating $p_{60,5}^{(H)}(s, K_5, k_5^{(H)})$. At the centroid of the cloud of dots, the percentage error is zero as the approximation is exact at $(\hat{K}_5, \hat{k}_5^{(H)})$. As the distance from the centroid increases, the percentage errors become higher. However, within the boundary of the cloud, the percentage errors are no greater than 0.01%, suggesting that the accuracy of the quadratic approximation is very high over the possible range of $(K_5, k_5^{(H)})$. Outside the boundary of the cloud, the percentage errors remain low.

We now move on to evaluating the linear approximation method for the situation when $u > t$ (Section 2.2.3). This approximation method is used when calculating $Q_t(t_0)$ and its derivatives, which are functions of $p_{x_f, t_0+T^*-1}^{(R)}(1, K_t, k_t^{(R)})$. In what follows we present the approximation results for this forward survival probability when it is evaluated at $x_f = 75$,

$t = t_0 = 5$ and $T^* = 10, 15, 20$.¹

The approximation results for the chosen values of x_f , t , t_0 and T^* are displayed in Figure A.2. As in Figure A.1, the left panels compare the actual and approximated values, while the right panels show the percentage errors. Within the region which the cloud of dots spans (i.e., possible values of K_5 and $k_5^{(R)}$), the percentage errors are generally less than 0.01%, indicating a very high degree of accuracy. Beyond the cloud's boundary, the accuracy of the approximation still remains satisfactory.

We have some additional comments on the left panels of Figure A.2. As lower values of K_5 and $k_5^{(H)}$ represent lower mortality, the value of the forward survival probability $p_{75,5+T^*-1}^{(R)}(1, K_5, k_5^{(R)})$ increases when the values of K_5 and $k_5^{(H)}$ decrease. However, the sensitivity to $k_5^{(H)}$ is inversely related to T^* , as indicated by the flattening of the contour lines when T^* increases. This observation offers an explanation as to why a q-forward with a longer time-to-maturity T^* is relatively more dependent on K_t (which affects both the q-forward and the pension plan) than $k_t^{(H)}$ (which has little effect on the pension plan) and hence provides a better hedge effectiveness.

¹The baseline results in Section 2.3 are generated under the assumption that $x_f = 75$. Also, because it is assumed that a freshly launched q-forward is written every time when the hedge is adjusted, we are particularly interested in the case when $t = t_0$.

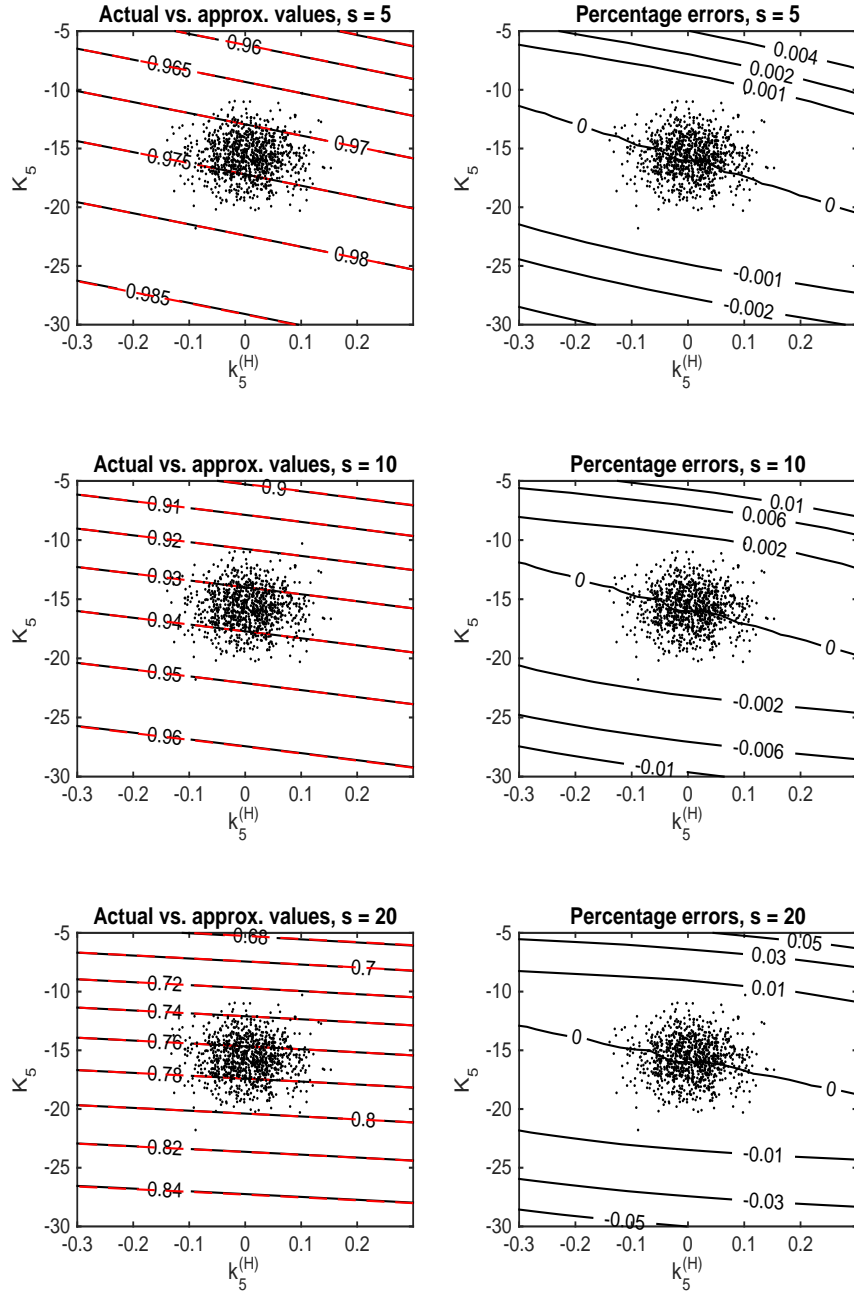


Figure A.1: Contour plots that show the degrees of accuracy in estimating $p_{x_0,t}^{(H)}(s, K_t, k_t^{(H)})$ for $t = 5$, $x_0 = 60$ and $s = 5, 10, 20$.

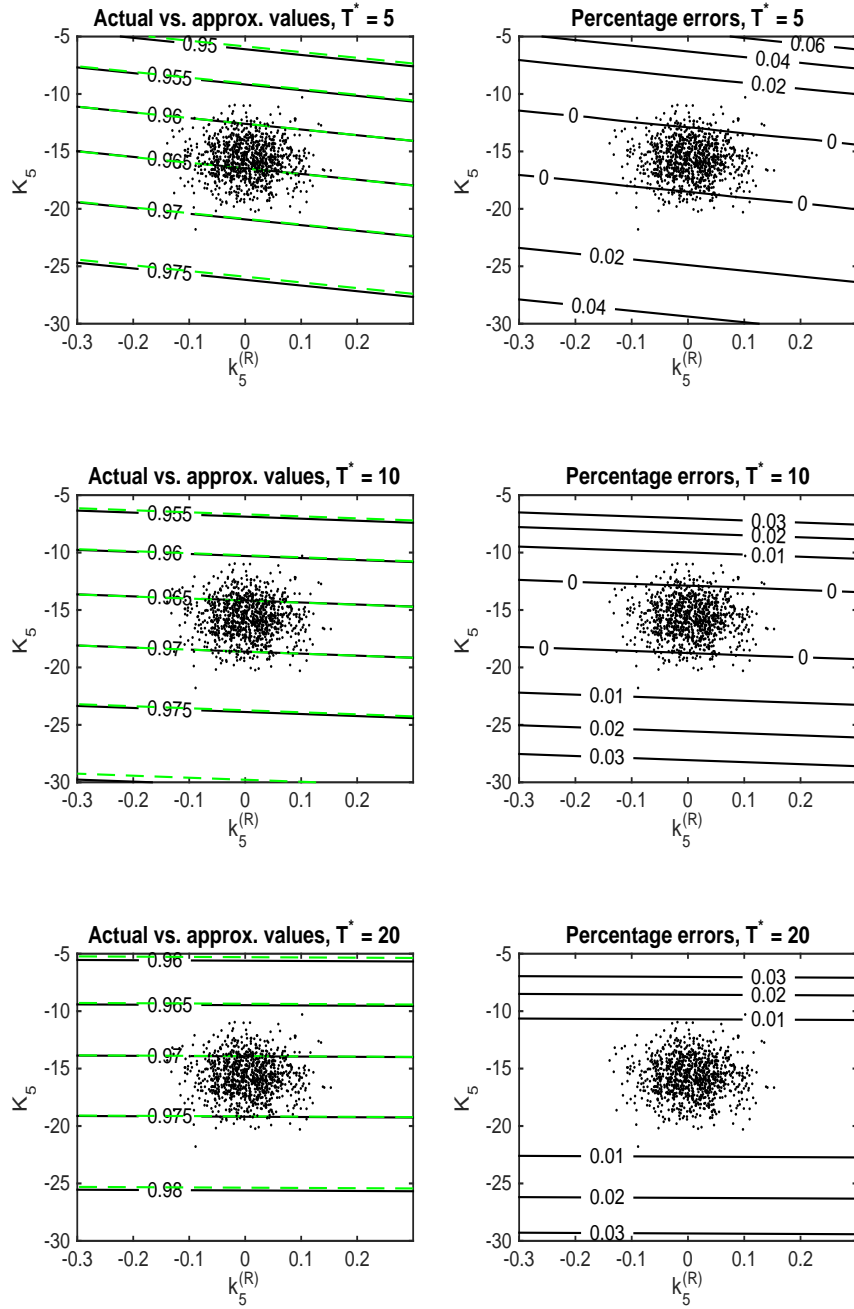


Figure A.2: Contour plots that show the degrees of accuracy in estimating $p_{x_f, t_0+T^*-1}^{(R)}(1, K_t, k_t^{(R)})$ for $x_f = 75$, $t = t_0 = 5$ and $T^* = 10, 15, 20$.

Appendix B

Deriving the Approximation Formula for $p_{x,u}^{(i)}(T, K_t, k_t^{(i)})$ when $u > t$

Let Z be a standard normal random variable that is independent of K_t and $k_t^{(i)}$. Using a first-order approximation, we have

$$\begin{aligned} p_{x,t}^{(i)}(T, K_t, k_t) &\approx \Phi(D_{x,t,0}^{(i)}(T) + D_{x,t,1}^{(i)}(T)(K_t - \hat{K}_t) + D_{x,t,2}^{(i)}(T)(k_t^{(i)} - \hat{k}_t^{(i)})) \\ &= \Pr(Z \leq D_{x,t,0}^{(i)}(T) + D_{x,t,1}^{(i)}(T)(K_t - \hat{K}_t) + D_{x,t,2}^{(i)}(T)(k_t^{(i)} - \hat{k}_t^{(i)}) | K_t, k_t^{(i)}) \\ &= \mathbb{E}(I_{Z \leq D_{x,t,0}^{(i)}(T) + D_{x,t,1}^{(i)}(T)(K_t - \hat{K}_t) + D_{x,t,2}^{(i)}(T)(k_t^{(i)} - \hat{k}_t^{(i)})} | K_t, k_t^{(i)}) \\ &= \mathbb{E}(I_{Z \leq D_{x,t,0}^{(i)}(T) + D_{x,t,1}^{(i)}(T)(K_t - \hat{K}_t) + D_{x,t,2}^{(i)}(T)(k_t^{(i)} - \hat{k}_t^{(i)})} | \mathcal{F}_t) \end{aligned}$$

where I_A is an indicator function which equals 1 if event A holds and 0 otherwise. The last step is due to the Markov property of the assumed stochastic processes for K_t and $k_t^{(i)}$.

For $u > t$, we have

$$\begin{aligned}
p_{x,u}^{(i)}(T, K_t, k_t^{(i)}) &= \mathbb{E}(p_{x,u}^{(i)}(T, K_u, k_u^{(i)}) | \mathcal{F}_t) \\
&\approx \mathbb{E}(\mathbb{E}(I_{Z \leq D_{x,u,0}^{(i)}(T) + D_{x,u,1}^{(i)}(T)(K_u - \hat{K}_u) + D_{x,u,2}^{(i)}(T)(k_u^{(i)} - \hat{k}_u^{(i)})} | \mathcal{F}_u) | \mathcal{F}_t) \\
&= \mathbb{E}(I_{Z \leq D_{x,u,0}^{(i)}(T) + D_{x,u,1}^{(i)}(T)(K_u - \hat{K}_u) + D_{x,u,2}^{(i)}(T)(k_u^{(i)} - \hat{k}_u^{(i)})} | \mathcal{F}_t) \\
&= \Pr(Z \leq D_{x,u,0}^{(i)}(T) + D_{x,u,1}^{(i)}(T)(K_u - \hat{K}_u) + D_{x,u,2}^{(i)}(T)(k_u^{(i)} - \hat{k}_u^{(i)}) | \mathcal{F}_t) \\
&= \Pr(Z - D_{x,u,0}^{(i)}(T) - D_{x,u,1}^{(i)}(T)(K_u - \hat{K}_u) - D_{x,u,2}^{(i)}(T)(k_u^{(i)} - \hat{k}_u^{(i)}) \leq 0 | \mathcal{F}_t).
\end{aligned}$$

Let $V_u^{(i)} = Z - D_{x,u,0}^{(i)}(T) - D_{x,u,1}^{(i)}(T)(K_u - \hat{K}_u) - D_{x,u,2}^{(i)}(T)(k_u^{(i)} - \hat{k}_u^{(i)})$. On the basis of the assumed stochastic processes, $K_u | \mathcal{F}_t$, $k_u^{(i)} | \mathcal{F}_t$ and thus $V_u^{(i)} | \mathcal{F}_t$ are normally distributed. It immediately follows that

$$p_{x,u}^{(i)}(T, K_t, k_t^{(i)}) \approx \Phi \left(\frac{-\mathbb{E}(V_u^{(i)} | \mathcal{F}_t)}{\sqrt{\text{Var}(V_u^{(i)} | \mathcal{F}_t)}} \right),$$

where

$$\begin{aligned}
\mathbb{E}(V_u^{(i)} | \mathcal{F}_t) &= -D_{x,u,0}^{(i)}(T) - D_{x,u,1}^{(i)}(T)(\mathbb{E}(K_u | \mathcal{F}_t) - \hat{K}_u) - D_{x,u,2}^{(i)}(T)(\mathbb{E}(k_u^{(i)} | \mathcal{F}_t) - \hat{k}_u^{(i)}) \\
\text{Var}(V_u^{(i)} | \mathcal{F}_t) &= 1 + (D_{x,u,1}^{(i)}(T))^2 \text{Var}(K_u | \mathcal{F}_t) + (D_{x,u,2}^{(i)}(T))^2 \text{Var}(k_u^{(i)} | \mathcal{F}_t) \\
&\quad + 2D_{x,u,1}^{(i)}(T)D_{x,u,2}^{(i)}(T) \text{Cov}(K_u, k_u^{(i)} | \mathcal{F}_t).
\end{aligned}$$

Under the assumed stochastic processes, we have

$$\begin{aligned}
\mathbb{E}(K_u|\mathcal{F}_t) - \hat{K}_u &= \mathbb{E}(K_u|K_t) - \mathbb{E}(K_u|K_0) \\
&= K_t + C(u-t) - K_0 - Cu = K_t - K_0 - Ct, \\
\mathbb{E}(k_u^{(i)}|\mathcal{F}_t) - \hat{k}_u &= \mathbb{E}(k_u^{(i)}|k_t^{(i)}) - \mathbb{E}(k_u^{(i)}|k_0^{(i)}) \\
&= (\phi_1^{(i)})^{u-t} k_t^{(i)} + \frac{1 - (\phi_1^{(i)})^{u-t}}{1 - \phi_1^{(i)}} \phi_0^{(i)} - (\phi_1^{(i)})^u k_0^{(i)} - \frac{1 - (\phi_1^{(i)})^u}{1 - \phi_1^{(i)}} \phi_0^{(i)} \\
&= (\phi_1^{(i)})^u ((\phi_1^{(i)})^{-t} k_t^{(i)} - k_0^{(i)}) + \frac{(\phi_1^{(i)})^u (1 - (\phi_1^{(i)})^{-t})}{1 - \phi_1^{(i)}} \phi_0^{(i)},
\end{aligned}$$

$$\text{Var}(K_u|\mathcal{F}_t) = \text{Var}(K_u|K_t) = \sigma_K^2(u-t),$$

$$\text{Var}(k_u^{(i)}|\mathcal{F}_t) = \text{Var}(k_u^{(i)}|k_t^{(i)}) = \frac{1 - (\phi_1^{(i)})^{2(u-t)}}{1 - (\phi_1^{(i)})^2} \sigma_{k,i}^2,$$

and $\text{Cov}(K_u, k_u^{(i)}|\mathcal{F}_t) = 0$.

Note that if a second-order approximation is used, then the derivation would require us to evaluate $\Pr(Z - D_{x,u,0}^{(i)}(T) - D_{x,u,1}^{(i)}(T)(K_u - \hat{K}_u) - D_{x,u,2}^{(i)}(T)(k_u^{(i)} - \hat{k}_u^{(i)}) - \frac{1}{2}D_{x,u,3}^{(i)}(T)(K_u - \hat{K}_u)^2 - \frac{1}{2}D_{x,u,4}^{(i)}(T)(k_u^{(i)} - \hat{k}_u^{(i)})^2 - D_{x,t,5}^{(i)}(T)(K_u - \hat{K}_u)(k_u^{(i)} - \hat{k}_u^{(i)}) \leq 0|\mathcal{F}_t)$, which cannot be accomplished analytically.

References

- Ahmadi, S. and Li, J.S.-H. (2014). Coherent mortality forecasting with generalized linear models: A modified time-transformation approach. *Insurance: Mathematics and Economics*, **59**, 194-221.
- Basel Committee on Banking Supervision (2013). Joint forum - Longevity risk transfer market: Market structure, growth drivers and impediments, and potential risks. Bank of International Settlements. Available at www.bis.org.
- Blake, D., Cairns, A.J.G., Coughlan, G., Dowd, K. and MacMinn, R. (2013). The new life market. *Journal of Risk and Insurance*, **80**, 501-557.
- Blake, D., Cairns, A.J.G. and Dowd, K. (2008). Longevity risk and the Grim Reaper's toxic tail: the survivor fan charts. *Insurance: Mathematics and Economics*, **42**, 1062-1066.
- Blake, D., MacMinn, R., Li, J.S.-H. and Hardy, M. (2014). Longevity risk and capital markets: The 2012-2013 update. *North American Actuarial Journal*, **18**, 501-557.

- Cairns, A.J.G. (2011). Modelling and management of longevity risk: Approximations to survival functions and dynamic hedging. *Insurance: Mathematics and Economics*, **49**, 438-453.
- Cairns, A.J.G. (2013). Robust hedging of longevity risk. *Journal of Risk and Insurance*, **80**, 621-648.
- Cairns, A.J.G., Blake, D. and Dowd, K., (2006a). A two-factor model for stochastic mortality with parameter uncertainty: Theory and calibration. *Journal of Risk and Insurance*, **73**, 687-718.
- Cairns, A.J.G., Blake, D. and Dowd, K. (2008). Modelling and management of mortality risk: A review. *Scandinavian Actuarial Journal*, **2008:2-3**, 79-113.
- Cairns, A.J.G., Blake, D., Dowd, K. and Coughlan, G.D. (2014). Longevity hedge effectiveness: A decomposition. *Quantitative Finance*, **14**, 217-235.
- Cairns, A.J.G., Blake, D., Dowd, K., Coughlan, G.D. and Khalaf-Allah, M. (2011). Bayesian Stochastic Mortality Modelling for Two Populations. *ASTIN Bulletin*, **41**, 29-59.
- Cairns, A.J.G., Blake, D., Dowd, K. and MacMinn, R., (2006b). Longevity bonds: Financial engineering, valuation, and hedging. *Journal of Risk and Insurance*, **73**, 647-672.
- Canadian Institute of Actuaries (2014). Final Report on Canadian Pensioners' Mortality. Available at <http://www.cia-ica.ca/docs/default-source/2014/214013e.pdf>.

- Chan, W.S., Li, J.S.-H. and Li, J. (2014). The CBD mortality indexes: modeling and applications. *North American Actuarial Journal*, **18**, 38-58.
- Chuang, S.-L. and Brockett, P.L. (2014). Modeling and pricing longevity derivatives using stochastic mortality rates and the Esscher transform. *North American Actuarial Journal*, **18**, 22-37.
- Continuous Mortality Investigation Bureau (2009). A prototype mortality projections model: Part two - detailed analysis. Continuous Mortality Investigation Working Paper 39.
- Coughlan, G.D., Khalaf-Allah, M., Ye, Y., Kumar, S., Cairns, A.J.G., Blake, D. and Dowd, K. (2011). Longevity hedging 101: A framework for longevity basis risk analysis and hedge effectiveness. *North American Actuarial Journal*, **15**, 150-176.
- Cox, S.H. and Lin, Y. (2007). Natural hedging of life and annuity mortality risks. *North American Actuarial Journal*, **11**, 1-15.
- Cummins, J.D. and Trainar, P. (2009). Securitization, insurance, and reinsurance. *Journal of Risk and Insurance*, **76**, 463-492.
- Dahl, M. (2004). Stochastic mortality in life insurance: Market reserves and mortality-linked insurance contracts. *Insurance: Mathematics and Economics*, **35**, 113-136.
- Dahl, M., Melchior, M. and Møller, T. (2008). On systematic mortality risk and risk minimization with mortality swaps. *Scandinavian Actuarial Journal*, **108**, 114-146.

- Dahl, M. and Møller, T. (2006). Valuation and hedging of life insurance liabilities with systematic mortality risk. *Insurance: Mathematics and Economics*, **39**, 193-217.
- Deng, Y., Brockett, P.L. and MacMinn, R.D. (2012). Longevity/mortality risk modeling and securities pricing. *Journal of Risk and Insurance*, **79**, 697-721.
- Dowd, K., Blake, D. and Cairns, A.J.G. (2010). Facing up to uncertain life expectancy: the longevity fan charts. *Demography*, **47**, 67-78.
- Dowd, K., Blake, D., Cairns, A.J.G. and Coughlan, G.D. (2011). Hedging pension risks with the age-period-cohort two-population gravity model. In: Seventh International Longevity Risk and Capital Markets Solutions Conference, Frankfurt, September 2011.
- Dowd, K., Cairns, A.J.G., Blake, D., Coughlan, G.D., Epstein, D. and Khalaf-Allah, M. (2011). A gravity model of mortality rates for two related populations. *North American Actuarial Journal*, **15**, 331-356.
- Fung, M.C., Ignatieva, K. and Sherris, M. (2014). Systematic mortality risk: An analysis of guaranteed lifetime withdrawal benefits in variable annuities. *Insurance Mathematics and Economics*, **58**, 103-115.
- Gatzert, N. and Wesker, H. (2010). The impact of natural hedging on a life insurer's risk situation. *The Journal of Risk Finance*, **13**, 396-423.
- Getmansky, M., Lo, A.W. and Makarov, I. (2004). An econometric model of serial correlation and illiquidity in hedge fund returns. *Journal of Financial Economics*, **74**, 529-609.

- Gnanadesikan, R. and Kettenring, J.R. (1972). Robust estimates, residuals, and outlier detection with multiresponse data. *Biometrics*, **28**, 81-124.
- Graziani, G. (2014). Longevity risk - A fine balance. *Institutional Investor Journals: Special Issue on Pension and Longevity Risk Transfer for Institutional Investors*, **2014**, 35-27.
- Haberman, S., Kaishev, V., Millosovich, P, Villegas, A., Baxter, S. Gaches, A., Gunnlaugsson, S. and Sison, M. (2014). Longevity basis risk: A methodology for assessing basis risk. Research investigation and report by Cass Business School and Hymans Robertson LLP for the Institute and Faculty of Actuaries and the Life and Longevity Markets Association. Available at <http://www.actuaries.org.uk/research-and-resources/documents/sessional-research-event-longevity-basis-risk-methodology>.
- Hatzopoulos, P. and Haberman, S. (2013). Common mortality modeling and coherent forecasts. An empirical analysis of worldwide mortality data. *Insurance: Mathematics and Economics*, **52**, 320-337.
- Human Mortality Database. University of California, Berkeley (USA), and Max Planck Institute of Demographic Research (Germany). Available at www.mortality.org or www.humanmortality.de (data downloaded on 1 April 2014).
- Idzorek, T.M., Xiong, J.X. and Ibbotson, R.G. (2012). The liquidity style of mutual funds. *Financial Analysts Journal*, **68**, 38-53.
- International Monetary Fund (2012). *Global financial stability report: the quest for lasting stability*, Washington, DC: International Monetary Fund.

- Jarner, S.F. and Kryger, E.M. (2011). Modelling adult mortality in small populations: The SAINT model. *ASTIN Bulletin*, **41**, 377-418.
- Lee, R. and Carter, L. (1992). Modeling and forecasting U.S. mortality. *Journal of the American Statistical Association*, **87**, 659-671.
- Lee, R. and Mason, A. (2010). Some macroeconomic aspects of global population aging. *Demography*, **47**, 151-172.
- Li, J.S.-H. and Hardy, M.R. (2011). Measuring basis risk in longevity hedges. *North American Actuarial Journal*, **15**, 177-200.
- Li, J.S.-H. and Luo, A. (2012). Key q-duration: A framework for hedging longevity risk. *ASTIN Bulletin*, **42**, 413-452.
- Li, J.S.-H., Ng, A.C.Y. and Chan, W.S. (2011). On the calibration of mortality forward curves. *Journal of Futures Markets*, **31**, 941-970.
- Li, N. and Lee, R. (2005). Coherent mortality forecasts for a group of populations: An extension of the Lee-Carter method. *Demography*, **42**, 575-594.
- Lin, T. and Tsai, C.C.L. (2014). Applications of mortality durations and convexities in natural hedges. *North American Actuarial Journal*, **18**, 417-442.
- LLMA (2012). Basis risk in longevity hedging: parallels with the past. *Institutional Investors Journal*, **2012**, 39-45.

- Lo, A., Petrov, C. and Wierzbicki, M. (2003). It's 11pm - do you know where your liquidity is? The mean-variance-liquidity frontier. *Journal of Investment Management*, **1**, 55-93.
- Loeys, J., Panigirtzoglou, N. and Ribeiro, R.M. (2007). Longevity: A market in the making. J.P. Morgan Research Paper. Available at <https://www.jpmorgan.com/directdoc>.
- Luciano, E., Regis, L. and Vigna, E. (2012). Delta-Gamma hedging of mortality and interest rate risk. *Insurance: Mathematics and Economics*, **50**, 402-412.
- Michaelson, A. and Mulholland, J. (2014). Strategy for increasing the global capacity for longevity risk transfer: Developing transactions that attract capital markets investors. *Journal of Alternative Investments*, **17**, 18-27.
- Ngai, A. and Sherris, M. (2011). Longevity risk management for life and variable annuities: The effectiveness of static hedging using longevity bonds and derivatives. *Insurance Mathematics and Economics*, **49**, 100-114.
- Ribeiro, R. and di Pietro, V. (2009). Longevity Risk and Portfolio Allocation. Available at <http://www.jpmorgan.com/pages/jpmorgan/investbk/solutions/lifemetrics/library>.
- Roxburgh, C., Lund, S. and Piotrowski, J. (2011). *Mapping global capital markets 2011*. McKinsey Global Institute. Available at <http://www.mckinsey.com/insights>.
- Skirbekk, V. (2004). Age and individual productivity: a literature survey. In Feichtinger, G. (ed.) *Yearbook of Population Research*, 133-153. Vienna: Austrian Academy of Sciences Press.

- Society of Actuaries. (2014). Mortality Improvement Scale MP-2014 Report. Available at <https://www.soa.org/Files/Research/Exp-Study/research-2014-mp-report.pdf>.
- Stevens, R. De Waegenaere, A. and Melenberg, B. (2011). Longevity risk and natural hedge potential in portfolios of life insurance products: The effect of investment risk. CentER Discussion Paper No. 2011-036.
- van Groezen, B., Meijdam, L. and Verbon, H. (2005). Serving the old: ageing and economic Growth. *Oxford Economic Papers*, **57**, 647-663.
- Wallis, K.F. (2003). Chi-Squared tests of interval and density forecasts, and the Bank of England's fan charts. *International Journal of Forecasting*, **19**, 165-175.
- Wang, J.L., Huang, H.-C., Yang, S. S. and Tsai, J.T. (2010). An optimal product mix for hedging longevity risk in life insurance companies: The immunization theory approach. *Journal of Risk and Insurance*, **77**, 473-497.
- Yang, S.S. and Wang, C.W. (2013). Pricing and securitization of multi-country longevity risk with mortality dependence. *Insurance: Mathematics and Economics*, **52**, 157-169.
- Zhou, R., Li, J.S.-H. and Tan, K.S. (2013). Pricing mortality risk: A two-population model with transitory jump effects. *Journal of Risk and Insurance*, **80**, 733-774.
- Zhou, R., Wang, Y., Kaufhold, K., Li, J.S.-H. and Tan, K.S. (2014). Modeling period effects in multi-population mortality models: Applications to Solvency II. *North American Actuarial Journal*, **18**, 150-167.